ABSTRACT

Title of Document: NA-ION INTERCALATED HIGHLY TRANSPARENT AND CONDUCTIVE FILMS

FENG GU, Master of Science, 2015

Directed By: Assistant Professor Liangbing Hu
Department of Material Science and Engineering

Transparent conductive films (TCFs) are materials with both high optical transmittance and high electrical conductivity. This thesis focuses on developing high transparent, high conductive, and low-cost transparent conductive films. This thesis reports Na-ion intercalated reduced graphene oxide (Na-RGO) films as low-cost, scalable, high performance transparent conductive films. The interlayer distance of RGO allows for Na-ion intercalation, which causes energy band structure changes and electron doping. As a result, a simultaneous increase in both transmittance and sheet conductivity has been achieved. The visible light transmittance and sheet resistance showed great enhancement from 36%, 83 kΩ/sq to 87%, 311 Ω /sq before and after Na-ion intercalation. The air stability test showed that the optical and electronic properties of Na-RGO films were more stable than Li-ion intercalated graphene. The results demonstrated the great potential of Na-ion intercalated printed RGO films for TCFs applications.

NA-ION INTERCALATED HIGHLY TRANSPARENT AND CONDUCTIVE FILMS

By

FENG GU

Thesis submitted to the Faculty of the Graduate School of the
University of Maryland, College Park, in partial fulfillment
of the requirements for the degree of
Master of Science
2015

Advisory Committee:
Assistant Professor Liangbing Hu, Chair/Advisor
Professor Lourdes G. Salamanca-Riba
Assistant Professor Yifei Mo

Dedication

To

My parents, Kaijin GU and Daomei Jiang

Acknowledgements

I would like to express my sincere gratitude to my advisor, Prof. Liangbing Hu for giving me the opportunity to work on exciting projects. I would especially like to thank for his support and guidance throughout my M.S. research at the University of Maryland. I benefited a lot from his guidance in many aspects during my M.S. study.

I would like to thank my committee members, Professor Lourdes G. Salamanca-Riba, Professor Yifei Mo for their invaluable advice.

Finally, I would also like to thank all previous and current members in Professor Hu Group, especially Jiayu Wan, for their help during my M.S. study in University of Maryland, College Park.

Table of Contents

List of Figures

Chapter 1: Introduction of Transparent Conductive Films

1.1 Background of Transparent Conductive Films Materials

1.1.1 Concept of Transparent Conductive Films

Transparent conductive films (TCFs) are materials that posses both high electrical conductivity and high optical transmittance in the visible spectral range [1]. TCFs play important roles in the information display and energy industries and are applied to a range of electronics, including solar cells [2], organic light-emitting diodes (OLED) [3], and touch screens [4] (Figure 1-1). To date, successful commercialized TCFs are mainly limited to Indium Tin Oxide (ITO) [5], although it has many shortcomings. With the increasing price of indium and demand for flexible consumer electronics in recent years, many emerging TCFs have been investigated as promising candidates. Currently, metal nanowires and carbon-based TCFs (including carbon nanotube, graphene, graphene oxide and reduced graphene oxide) hold the most promise for next generation transparent conductive films. However, these candidates all have their own advantages and disadvantages.

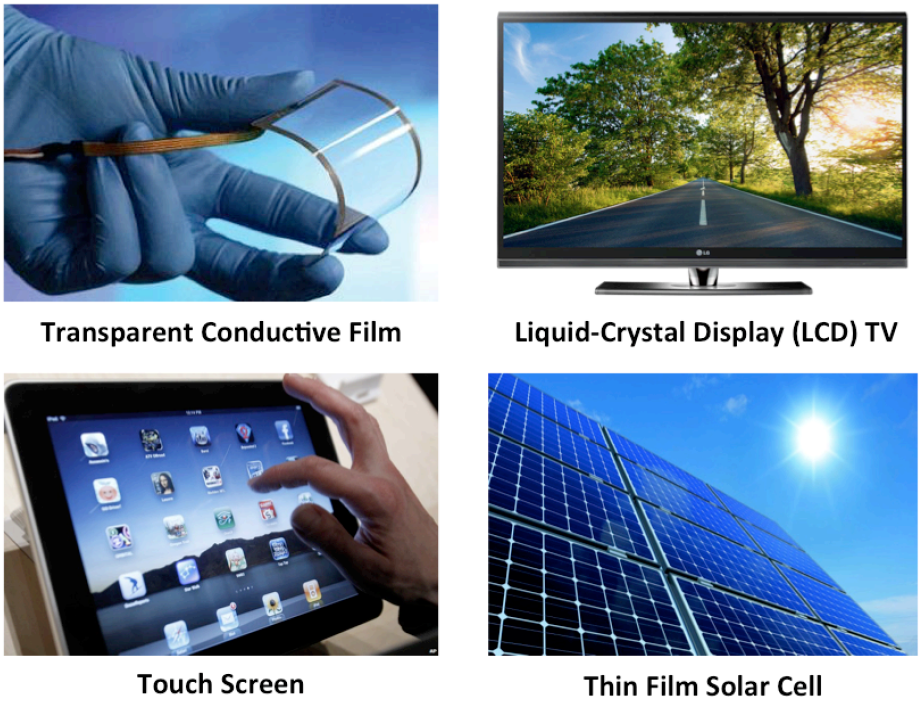

Figure 1-1. Transparent conductive film and its applications.

1.1.2 Fundamentals about Transparent Conductive Films

There are many factors influencing the performance and choice of TCFs, including cost, toxicity, air stability, thermal durability, thickness, flexibility, physical and chemical stability, plasma wavelength, work function, and uniformity. Among these considerations, the most critical requirements for TCFs are high transmittance and high conductivity, which normally have an inverse relationship. Materials with a high conductivity σ usually have a high carrier concentration n (electrons) and high carrier mobility $\mu_{n,p}$ as well, according to equation: $\sigma = en\mu_{n,p}$ [6] the e is elementary charge. Electrons have a smaller effective mass than ions, which gives them more mobility μ. Therefore, electrons will act as charge carriers in conductive electrodes. The product of carrier concentration n and carrier mobility $\mu_{n,p}$

maximizes conductivity σ. For semiconductors, the carrier concentration n is decided by the amount of electronically active dopant, which could be placed in the lattice [7]. For metals, the carrier concentration n is decided by the structure of the metal.

Meanwhile, the absorption of light by electrons (carriers) holds the limit to the carrier concentration n. From the plasma oscillation resonance or plasmon [8] formed by carrier electrons, plasma frequency is given by (1): $\omega_p = \sqrt{\frac{ne^2}{m^*\varepsilon_r\varepsilon_0}}$ [9]. The m* is effective mass of the carriers (electrons), $\varepsilon_r\varepsilon_0$ is the permittivity of material. $E_p = c\omega_p$ is the energy of the plasmon, c is the speed of light, and $\lambda_p = \frac{2\pi\hbar}{\omega_p}$ is the wavelength of the plasmon. Here the plasma frequency plays a vital role in TCFs. If the plasma frequency of the TCFs is higher than the frequencies of the light, the electrons won`t be excited and the TCFs acts as a transparent dielectric [7]. If the frequencies of the light were lower than the plasma frequency, the TCFs would reflect and absorb incident light. Therefore, for TCFs, the plasma frequencies should be in the transparent frequency light range.

1.1.3 Standard for Transparent Conductive Films

Besides the standards discussed above, there are two important parameters for TCFs, the optical transmittance (T) at visible light and the electrical sheet resistance (R_S). Researchers derived a more comprehensive criterion——the figure of merit (FOM). The FOM combines both properties of optical transmittance (T) (usually measured under 550nm wavelength) and electrical sheet resistance (R_S). The equation

(2) is: $T = \left(1 + \frac{188.5}{R_{sh}} \cdot \frac{\sigma_{OP}}{\sigma_{DC}}\right)^{-2}$ [10]. The σ_{OP} is the optical conductivity and σ_{DC} is the DC conductivity of the material. Therefore, from fundamental level, the FOM is characterized by the ratio of $\frac{\sigma_{DC}}{\sigma_{OP}}$, which combines transmittance and conductivity properties. The higher the FOM is, the better the TCFs will be.

1.2 Current and Promising Transparent Conductive Films

TCFs materials can be classified into three categories according to the carrier concentration n, which determines both optical and electrical properties. The first category is transparent conductive oxides (TCOs), such as indium tin oxide (ITO). TCOs have high mobility μ and high carrier concentration n $\approx 10^{21} cm^{-3}$ [11]. The second category is metal grid or metal nanowire, such as silver nanowire (AgNW). They also have high carrier mobility μ, high carrier concentration n$> 10^{22} cm^{-3}$. The third category is carbon-based materials, which include carbon nanotubes, graphenes and reduced graphene oxides. They have low carrier concentration n $\approx 10^{20} cm^{-3}$ and low mobility μ.

1.2.1 Transparent Conductive Oxides

To date, the most commercially successful transparent conductive oxide (TCO) for TCFs is ITO (Figure 1-2). However, ITO was applied as low-emissivity coating for glass [12] when they first appeared, which is an approach for the energy efficiency improvement for the 1970s oil crisis. ITO has a bandgap of 3 eV, making it suitable for applications in the visible light range [13]. ITO has the carrier

concentration n of $10^{20} cm^{-3}$ *to* $10^{21} cm^{-3}$ the electron mobility of 10 *to* $30\ cm^2 V\ s$ [14], and low resisitivity (at the range of $10^{-4} \Omega/cm$ with as high as 92% transmittance) [15]. Current commercially available ITO has good optical and electrical properties with typical values of 80% transmittance at 10 Ω/sq [16], which allowed it to dominate the TCFs market for several decades. However, with expanding demand for optoelectronics, the scarcity of indium (main material for ITO) limits future growth. Moreover, ITO is a brittle material, which is not suitable for the current trend of flexible electronics. Compared to the roll-to-roll fabrication process of other TCFs, the sputter deposition process costs much more.

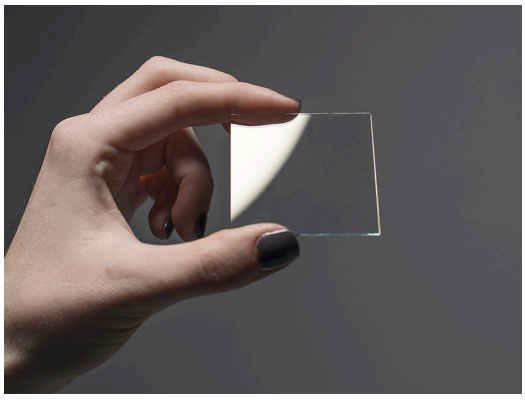

Figure 1-2. ITO coated glass substrate. Adapted from www.adafruit.com.

Other TCOs, such as aluminum-doped ZnO (AZO), have also been studied. *Minami* [11] reported that the AZO films have the potential to be a promising candidate for TCFs. AZO has a low resistivity of the order of $10^{-5} \Omega/cm$ and consists of cheap and non-toxic source materials. However, one major problem for AZO film is its electrical instability in air [17]. In sum, due to the disadvantages discussed above, researchers have been looking for alternative materials.

1.2.2 Metal Nanowires

Alternatives for TCFs include metal grids or metal nanowire networks. Silver nanowire (AgNW) stands out as the most investigated candidate. *Hu* [18] reported an 87% transmittance with 20 Ω/sq of AgNW film with the Meyer rod coating method. *Sepulveda-Mora* [19] reported an 89.9% transmittance with 10.2 Ω/sq AgNW thin films by a simple dip-coating [20] technique and a subsequent annealing step (Figure 1-3). Nevertheless, some problems still hinder its practical applications. The percolation [21] and contact resistance between nanowires are the intrinsic problems to be solved. Also, high uniformity, scalable fabrication and long-term stability are problems that have not been addressed. Investigators also studied other metal nanowire for flexible transparent conductive electrodes, i.e. copper nanowires (CuNW). *Rathmell* [22] reported a 15 Ω/sq with 61% transmittance for CuNW films. Although CuNW remained air-stable for one month and no change in sheet resistance after bending test, the low transmittance is still a major problem in optoelectronics applications.

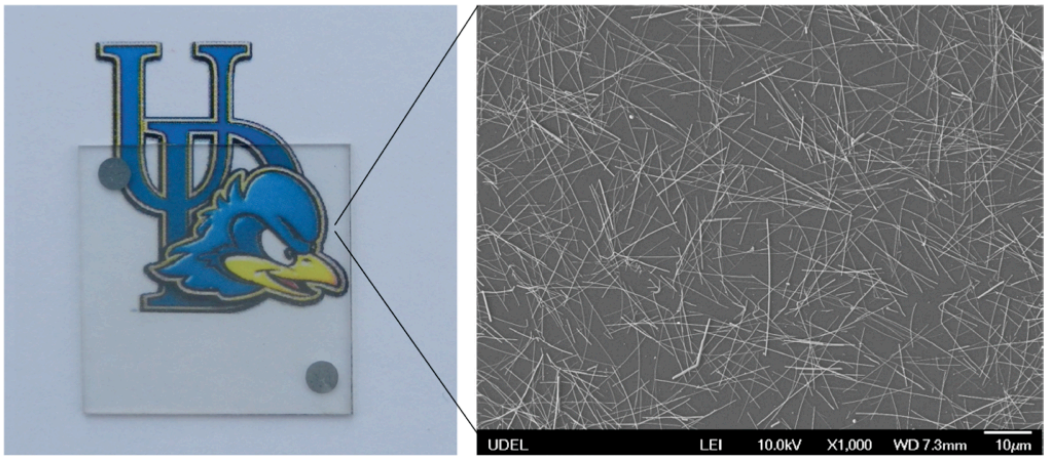

Figure 1-3. Silver nanowire transparent conductive film (left) and SEM image of the same film (right). Adapted from ref. [19].

1.2.3 Carbon-based TCFs

Carbon-based TCF materials are an emerging class of candidates, which include carbon nanotube (CNT), graphene, and reduced graphene oxide (RGO).

Carbon Nanotube (CNT)

CNT TCFs have several advantages over ITO. There are multiple methods available for CNT TCFs fabrication, such as casting [23], spin coating [24], dip coating, Meyer rod coating [25], and vacuum filtration followed by transfer [26], and most of them are scalable. Also, the CNT TCFs are printed out of solution-based CNT ink, and only small amounts of CNT ink are required for printing. As a promising alternative for ITO, CNT-based TCFs have been investigated a great deal. *Hecht* [27] reported a sheet resistance of 60 Ω/sq with 90.9% transmittance of CNT transparent conducting film deposited on a substrate surface (Figure 1-4). Though the performance of CNT TCFs is satisfying, commercialization problems still exist. One typical problem is the purity of the CNT ink. Since the production of CNT normally contains impurities, such as a catalyst, there should be a sufficient enough way to purify CNT ink. Also, better dispersion processes for stable CNT inks with better CNT dispersion is required. Furthermore, significant improvement has to take place to reduce the CNT-CNT junction resistance.

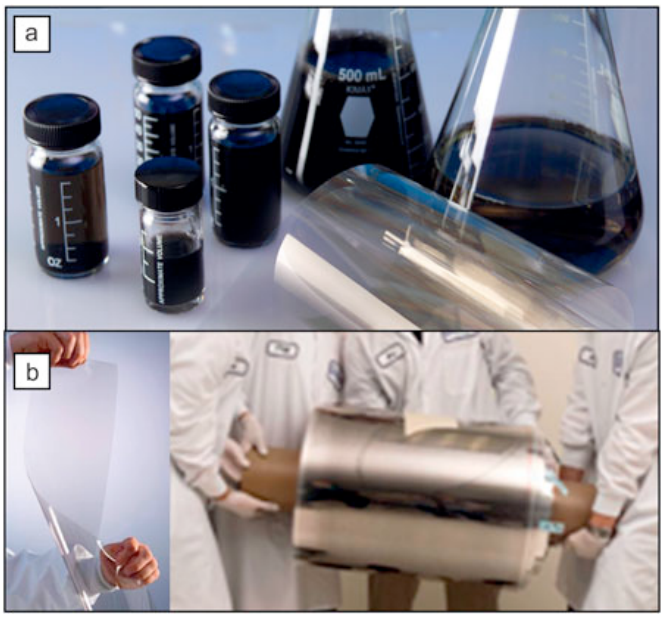

Figure 1-4. Carbon nanotube (CNT) ink and CNT film. (a) CNT ink. (b) A piece of CNT film on PET substrate (left); A roll of CNT film (right). Adapted from ref. [27].

Graphene-based TCFs

Graphene is a single atomic layer of graphite, an abundant, allotropic carbon material, made of tightly trigonally bonded sp^2 carbon atoms with a honeycomb lattice structure. Since this 2D material was isolated in 2004 [28] and win the 2010 Nobel Prize in Physics, it continues to exhibit amazing properties and draw much attention from many aspects: mechanical properties of 130 Gpa intrinsic strength and 1 TPa Young`s Modulus [29]; optical property of 97.7% transmittance (2.3% optical absorption) [30]; thermal conductivity of 3000 W/mK [31]; electronic property of ~ $5\times10^3 cm^2V^{-1}s^{-1}$electron mobility at room temperature [32]. Also, graphene has the ability to sustain extremely high current density compared to copper [33]. And another amazing property is that graphene can readily be chemically functionalized

[34] into GO (graphene oxide) or even further RGO (reduced graphene oxide), which are hydrophilic (Figure 1-5).

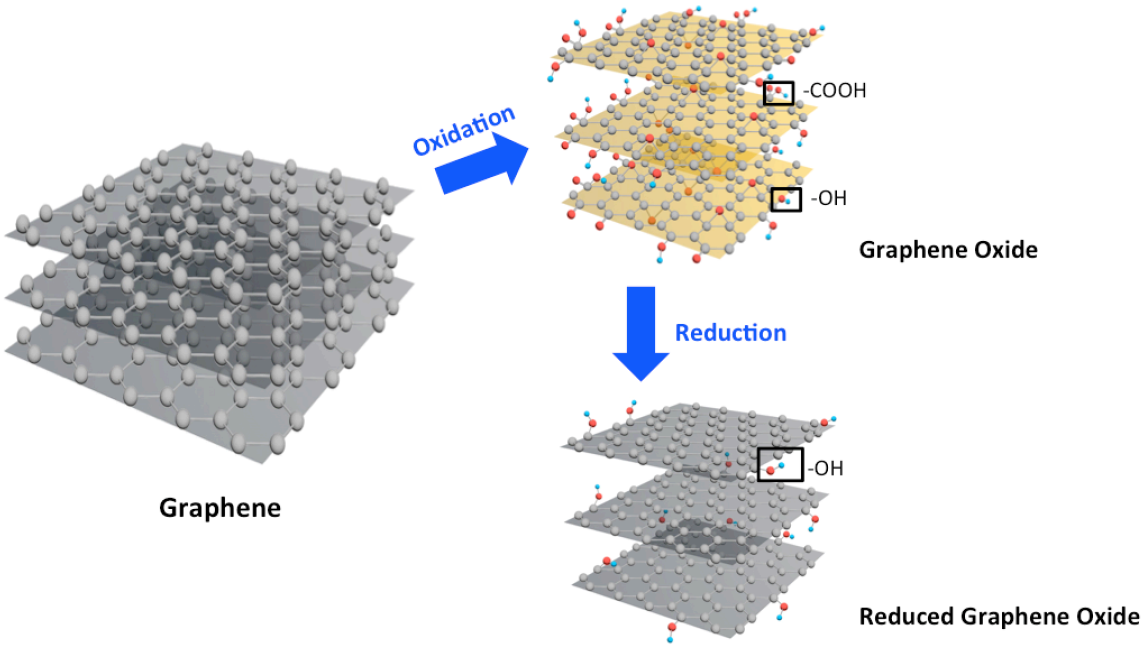

Figure 1-5. Schematic structures of graphene, GO and RGO.

Among these properties, the high transmittance and high electron mobility of graphene have attracted much attention in TCFs application. *Bonaccorso* [35] reported an equation to define the relation between transmittance T and sheet resistance R_S for few layer graphene films: $T=\left(1+\frac{Z_0}{2R_s}\frac{G_0}{\sigma_{2D}}\right)^{-2}$. Z_0 is the free-space impedance, G_0 is the optical conductivity and $\sigma_{2D} = n\mu e$ for graphene. Ideally, intrinsic single layer graphene has a performance of 6 Ω/sq sheet resistance at 97.7% transmittance. Steady progress has been made to improve the performance, including spin coating [36], dip coating [2], roll-to-roll [4], vacuum filtration [37], and chemical vapor deposition (CVD) [38]. For example, the roll-to-roll processed graphene

transparent films have been demonstrated with a performance of 30 Ω/sq sheet resistance at 90% transmittance [4] (Figure 1-6). More recently, people have studied chemical doping method for improving performance of graphene-based TCFs. Ferric chloride (FeCl3) intercalated in few-layer graphene (FLG) has shown a sheet resistance of 8.8 Ω/sq at 84% transmittance [39]. Recently, *Bao* [40] reported a sheet resistance of 3.0 Ω/sq at 91.1% transmittance with lithium ion (Li-ion) intercalated FLG. Though the performance is good enough for optoelectronic devices, these materials are not cost-effective and scalable enough for commercialization level.

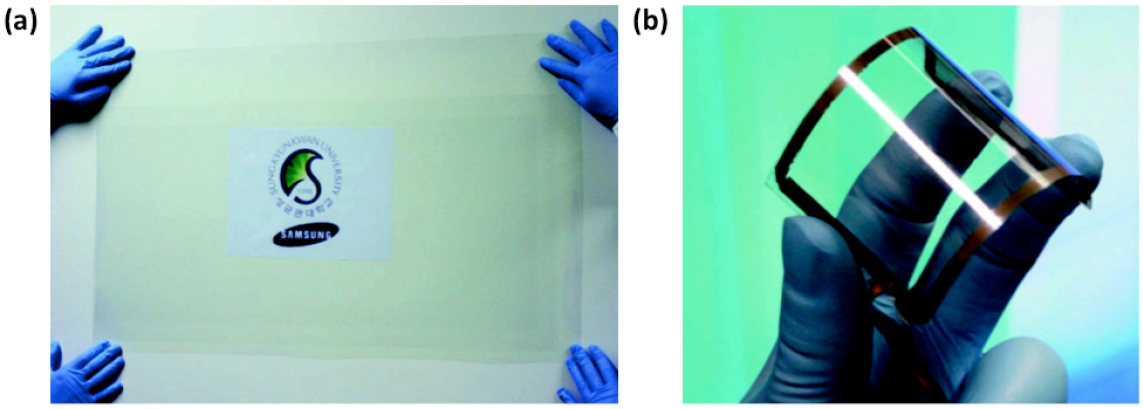

Figure 1-6. Transparent graphene film and graphene-based touch panel. (a) A transparent graphene film on a 35-inch PET substrate. (b) Aassembled touch panel with graphene/PET. Adapted from ref. [4].

Reduced Graphene Oxide (RGO) TCFs

Graphene oxide (GO) is a hydrophilic nanomaterial oxidized from graphite with extensive chemical exfoliation. However, the oxidization introduces oxygen functional groups into the pristine graphene structure, including hydroxyl, carbonyl, carboxylic and epoxy (1,2-ether) functional groups. These groups break down the

long-range conjugated network of graphene [41], which result in a decrease in both carrier concentration and mobility. The removal of these groups with a reduction process thermally or chemically could enhance the electrical conductivity of GO. Though the electrical properties are not comparable with pristine graphene, the solution-based and cost-effective process still makes reduced graphene oxide (RGO) attractive for large-scale applications. So far, RGO films made from GO have been reported with a sheet resistance of 840 Ω/sq at 78% transmittance [42] (Figure 1-7). *Hwang* [43] reported a sheet resistance of 300 Ω/sq at 80% transmittance for N-doped RGO films. Though the performance is not comparable to ITO, these findings suggest the possibility of RGO-based film as a scalable candidate for TCFs applications.

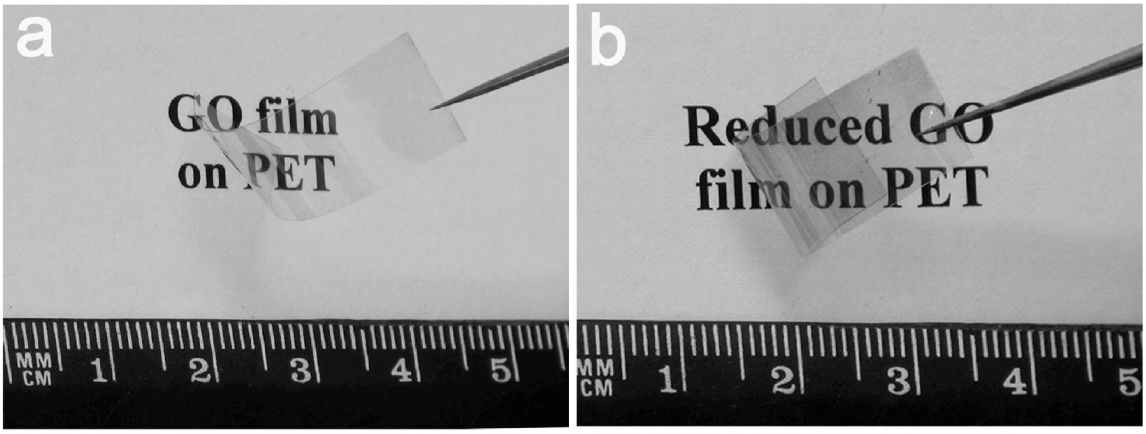

Figure 1-7. Optical images of GO film and RGO film. (a) GO film before HI acid reduction. (b) RGO film (GO film after HI acid reduction). Adapted from ref. [42].

1.3 Motivations and Objectives of This Research

1.3.1 Motivations

Chemical doping [4] has been studied for enhancement of electrical and optical properties. The p-doped four-layer graphene has ~30 Ω/sq at ~90% transmittance. Chemical intercalation also has been reported. *Khrapach* [44] reported few-layer graphene intercalated with ferric chloride ($FeCl_3$) to be an effective method to enhance electrical conductivity while maintaining high transmittance; it has a performance of 8.8 Ω/sq at 84% transmittance. Intercalation has been reported as a potential approach to increasing carrier density, which contributes to lowering the sheet resistance and increasing the optical transmittance; a recent publication reported an approach of electrochemical Li-ion intercalation improved FLG TCFs, which resulted in a synergic enhancement of optical transmittance and electrical conductivity [40]. The major reason for this is that the heavily doped Li-ions shifted up the Fermi level of FLG, which increases carrier density. The increased Fermi energy results in suppression of interband optical transitions for photon energy, which increases transmittance and decreases optical conductivity [40]. Also, high Li-ion doping level of FLG likely causes the reduction of conductivity, which is shown in the sheet resistance of LiC_6 (Li-ion intercalated FLG). However, the Li-ion intercalation encountered an air-stability issue that could limit its application.

In this work, RGO film and Na-ions intercalants were used instead of graphene and Li-ions intercalants for transparent films. The main reasons for the use of RGO film and Na-ions can be explained as follows. Compared to graphene flakes or CVD

graphene, the RGO films fabricated in this study are solution-based, which is printable and more scalable. Also, due to the abundant source of sodium, the price of sodium (Na) is much lower than lithium (Li). Therefore, the total cost has been reduced greatly for large-scale TCFs applications from these aspects. Besides the cost-related advantage, there is another motivation for the use of Na-ions as intercalants. According to the experiment, Na-ions could form a more stable barrier layer than Li-ions, which could avoid further oxidation and side effects. Unlike Li-ions, Na-ions can`t intercalate into graphene due to its small interlayer distance. However, Na-ions can intercalate into RGO, which will be discussed later in details.

1.3.2 Objectives of This Research

This thesis focuses on Na-ion intercalated high transparent and conductive films with a printed reduced graphene oxide (RGO) film based on the recent publication [45]. Compared to Li-ion intercalated few-layer graphene; there are several major motivations. The larger interlayer distance of RGO would easily allow for Na-ion intercalation [46]. RGO has a relatively larger flake size than graphene, which could provide better junction contact [42]. A drastic enhancement of optical transmittance from 36% to 79% and a decrease in sheet resistance from 83 kΩ /sq to 311 Ω /sq has been obtained with Na-RGO films. This performance stands out among previous reported RGO-based TCFs in publications. Also, the Na-RGO film showed a much better air-stability. Therefore, Na-RGO film exhibits great potential as a candidate for TCFs. Besides, the fabrication process is mainly solution-based and very scalable.

Chapter 2: Fabrication of Na-RGO Films

2.1 Na-ion Intercalated Printed RGO Films

2.1.1 Graphene Oxide Preparation

Graphene oxide (GO) ink was prepared by improved Hummer`s method [47] with natural graphite flakes (Sigma-Aldrich, cat #332461, ~150 μm flakes). Figure 2-1(a) shows the graphite flakes. A 9:1 volume ratio mixture of concentrated H2SO4 acid (180 ml) and concentrated H_3PO_4 acid (20 ml) was mixed together. The mixed acid was poured slowly into the mixture of 1.5 g natural graphite flakes and 7.2 g $KMnO_4$ in a flask. The solution was kept at 50 °C with water bath and stirred for 12 hours with a stirrer with the speed of 250 rpms (Figure 2-1(b)). The reactant was cooled down to room temperature and then was mixed with 500 ml ice (made from deionized water) and H_2O_2 (3 mL) in a beaker. Stir the liquid mixture until it cooled down to room temperature again. Figure 2-1(c) shows that the centrifuge was working to wash away H_2SO_4/H_3PO_4 acid and $KMnO_4$ with deionized water with a speed of 6000 rpm, 15 minutes for 3 times. Take the remaining solid reactants (basically graphene oxide) out and pour them into a clean beaker. Add 200 ml 30% dilute HCl acid to expand the thick graphene oxide flakes. The graphene oxide (GO) was washed for several times with deionized water and centrifuge the ink at 8000 rpm for several hours until the Cl^- ions were washed away. In figure (d) as prepared GO solution is at a concentration of 5 mg/mL.

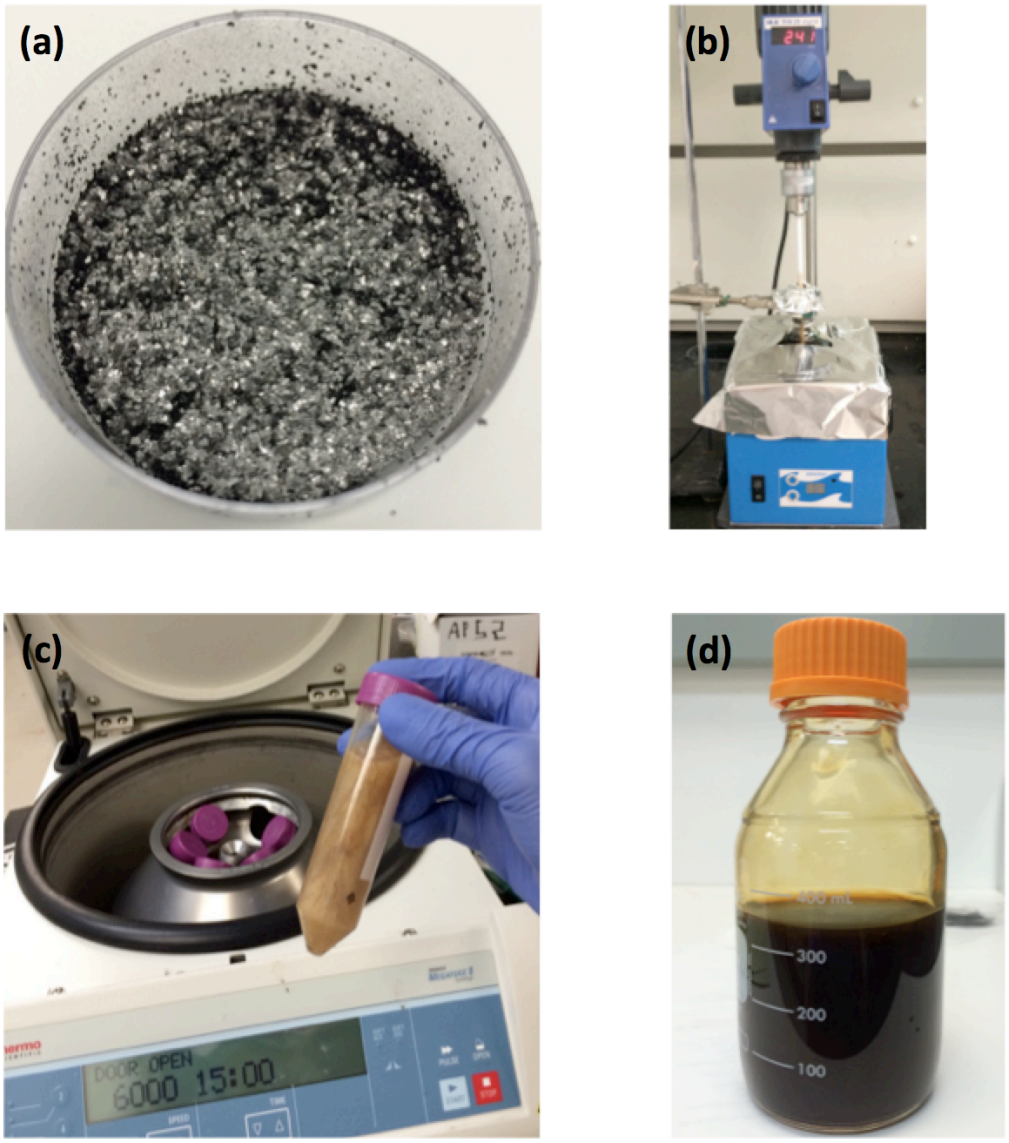

Figure 2-1. Graphene oxide ink fabrication process. (a) Natural graphite flakes. (b) The mixture reactant of strong acid, KMnO4 and graphite flakes was kept at 50 ℃ with water bath and stirred for 12 hours. (c) The mixture solution was centrifuged for purification. (d) As prepared GO ink.

2.1.2 RGO Film Preparation

In Figure 2-2(a), a mixed solution of Zonyl and GO (w:w=3:10) is then prepared for coating. 150μL GO ink was dropped at the edge of one clean glass slide with pipette followed by Meyer rod (R.D. Specialties, #10) coating process. In Figure 2-2(b), the glass substrate surface was uniformly coated with GO ink, then it was dried with a hot plate at 50 °C for 1 min. This step was repeated for several times until a required GO film thickness was achieved. The coated GO film glass slides were reduced in a tube furnace under reduction atmosphere with controlled flowing Ar/H_2 (95%/5 %) gas. The GO films were annealed and heated up with a heating rate of 1 °C/min from room temperature to 300 °C. After the samples were cooled down to room temperature from 300 °C in furnace, the RGO films were ready [45].

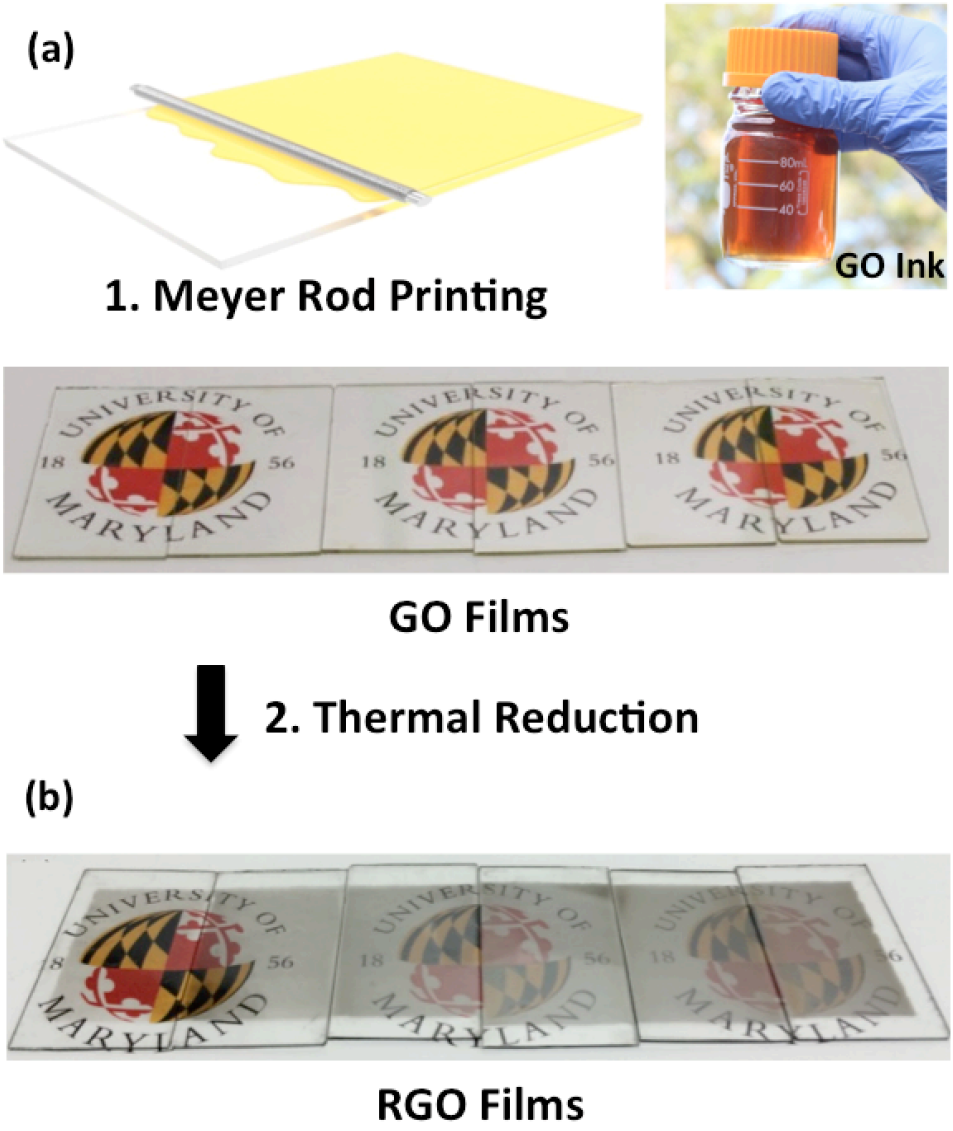

Figure 2-2. RGO films fabrication process. (a) A bottle of prepared GO ink for printing. (b) Meyer-rod printing of GO ink with excellent uniformity on glass substrate. (c) RGO films after thermal reduction in tube-furnace under reduction atmosphere. Figures adapted from ref. [45].

The Meyer rod coating method is used for GO coating. Besides the uniform coating of GO and annealed RGO films shown in Figure 2-3(c), the thickness is also

controllable. The thickness of the RGO film is measured by AFM. Further plot the thickness of the RGO film is shown in Figure 2-3(b-g). A minimum RGO thickness of 13.5 nm is achieved by one time Meyer rod coating (GO solution concentration is 2 mg/mL). A change of Meyer rod size and a decrease concentration of GO solution will also lead to a thinner RGO thickness. Technically, monolayer GO coverage can be achieved by Meyer rod method. Since the RGO film needs to be conductive in order for Na-ion intercalation, 4-5 layers of coating (GO concentration of 2 mg/mL) result to an optimized thickness.

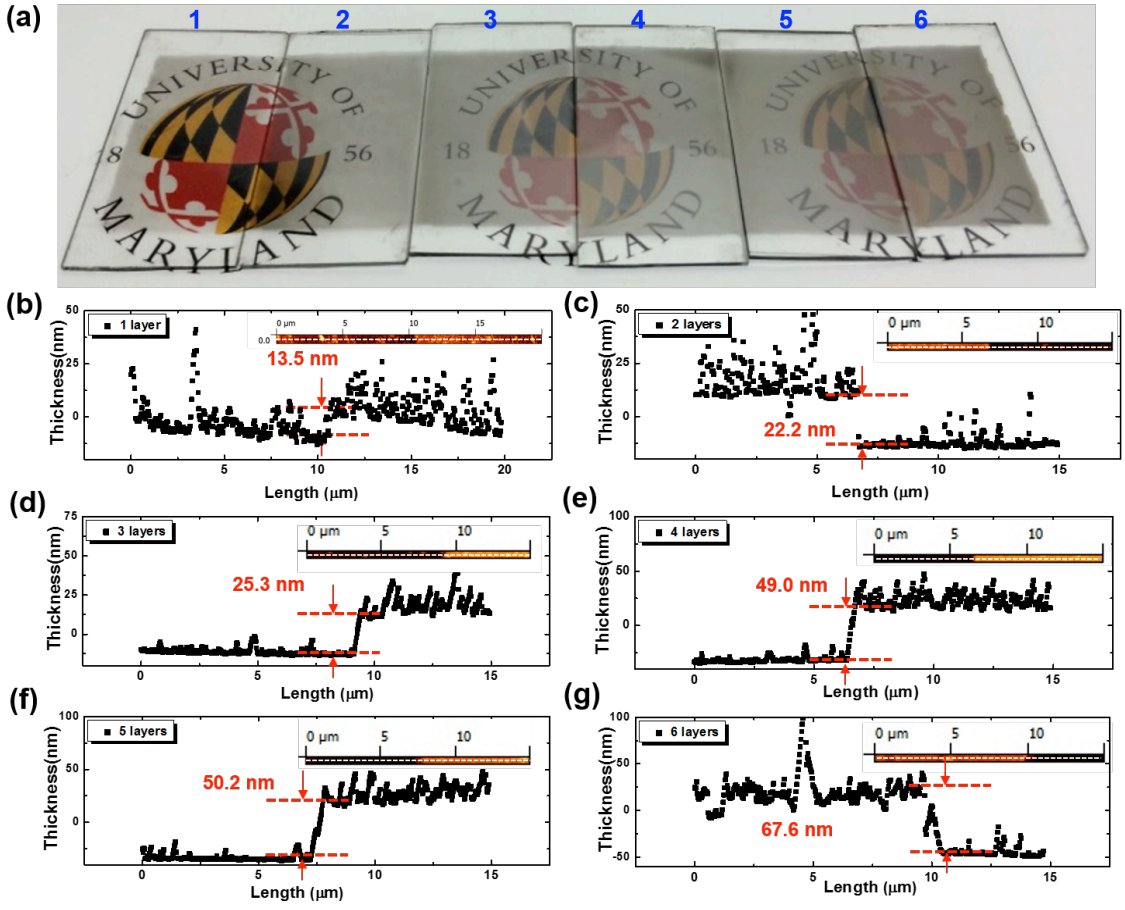

Figure 2-3. Controllability for thickness of RGO films. (a) RGO on glass substrates with 1 to 6 times of Meyer rod coating of GO ink. (b-g) Thickness of the 1-6 times coated RGO films by AFM measurement.

2.1.3 RGO Film Planar-battery Fabrication

The RGO films on glass substrate were tailored with blades into designed shape and size according to the designed pattern. In Figure 2-4(a), with physical vapor deposition method, the copper electrodes were deposited on the RGO film target with a designed mask pattern. And PDMS (Polydimethylsiloxane) frameworks were set up on copper electrodes and wires were then soldered on the copper electrodes. After these processes, the whole devices were taken into glove box for Na metal deposition and liquid electrolyte ($NaPF_6$ in EC: DEC, v:v=1:1) addition. In figure (b), the device was sealed with epoxy glue and a glass substrate cover inside the glove box. Connect the wires of the device outside the glove box to the battery tester to apply current for Na-ions intercalation [45].

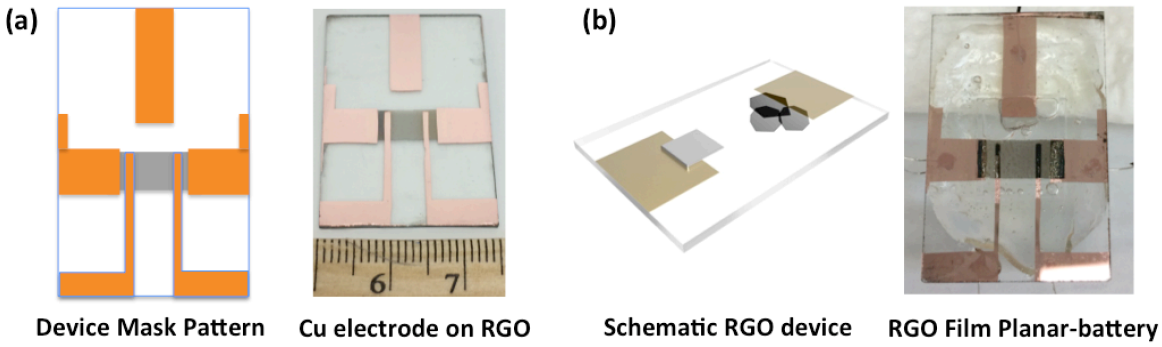

Figure 2-4. RGO planar-battery fabrication process. (a) Device mask pattern and physical vapor deposited copper electrode on target RGO film. (b) Schematic and real image of RGO film device with copper as working electrode, Na metal as the anode and 1M NaPF6 in EC: DEC (1:1=v:v) as electrolyte.

2.2 Optical Transmittance and Sheet Resistance Measurement

As illustrated above in Figure 2-5(a), Na-RGO films were achieved by applying a current with a battery tester (Bio-logic USA) on the prepared RGO device with the RGO and Na metal. After applying the potential, Na-ions would start to intercalate into the RGO film. Before and after the Na-ion intercalation, the optical transmittances of RGO/Na-RGO films were obtained by calculating the grey scale image taken by the charge-coupled device (CCD), which was coupled to a microscope (Nikon Eclipse Ti-U) in transmission mode. To obtain transmittance at 550 nm (common wavelength for TCFs transmittance measurement), a narrow-band filter (Thorlabs Inc.) was used in the optical path [45].

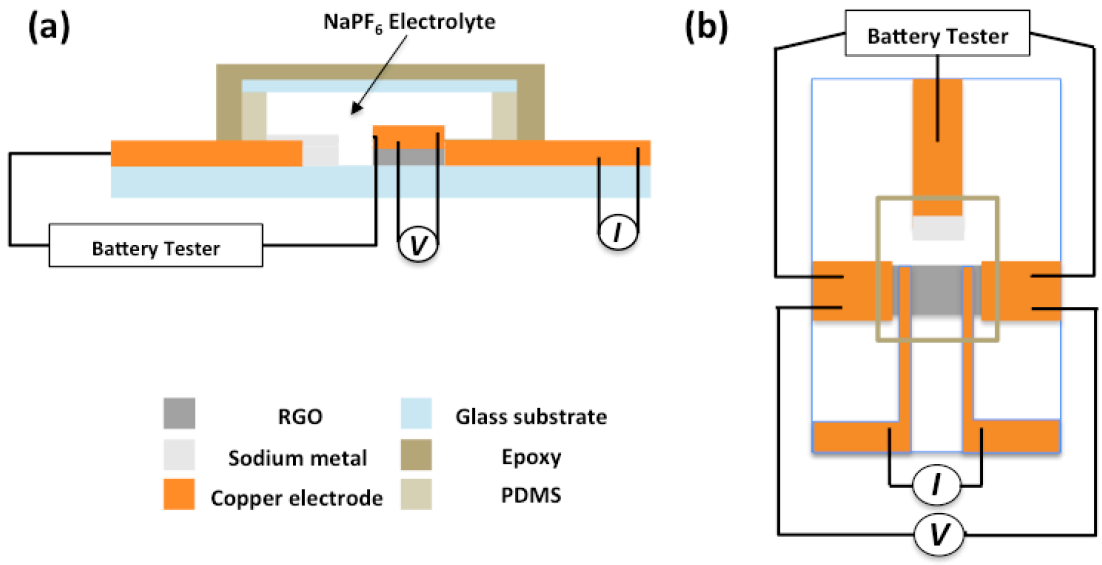

Figure 2-5. Sheet resistance measurement set-up. (a) and (b) are schematic side view and vertical view of In-situ sheet resistance measurement for Na-ion intercalated RGO with the planar battery device, respectively.

For the electrical conductivity, the sheet resistance of the Na-RGO films was measured with a four-probe method (Figure 2-5). There is a 5 mm x 5 mm square RGO area for testing. Figure (a) and (b) are schematic structures of the side view and vertical view for In-situ sheet resistance measurements set-up, respectively. With this method and the planar battery device, the sheet resistance can be measured while the battery tester is applying the potential to the device.

2.3 RGO Coin Cell Fabrication

To demonstrate Na-ions can intercalate into RGO, a coin cell was made with freestanding RGO film as a cathode, and Na metal as anode. First, the GO film was vacuum-filtrated with GO ink. Then, the GO film was reduced in tube furnace under a reduction atmosphere of controlled flowing Ar/H_2 (95%/5 %) gas at the speed of 1 ˚C/min from room temperature to 300 ˚C. Then as the prepared freestanding RGO film was taken out from tube furnace and assembled into a coin cell in glove box. After cycling the cell with a battery tester, the RGO freestanding film became Na-RGO freestanding film. Disassemble the coin cell and put the Na-RGO film in sealed plastic wrap in Argon-filled exchange box before X-Ray Diffraction characterization.

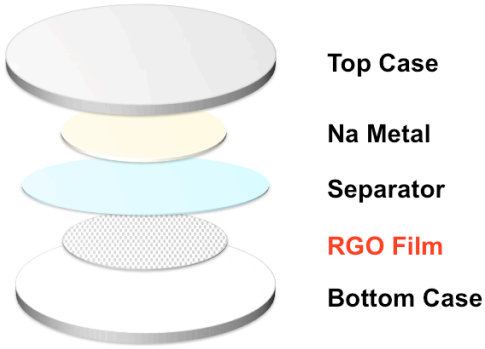

Figure 2-6. RGO coin cell set-up

Chapter 3: Na-RGO Transparent Conductive Films

3.1 Principle of Na-ion Intercalation for RGO Films

Figure 3-1(a-b) schematically shows the Na-ions intercalation process for RGO film. The Na-ion intercalation would enhance optical transmittance and electrical conductivity of the RGO film, simultaneously. This process was achieved by applying a current source with a battery tester (Bio-logic USA) between the printed RGO film target (as cathode) and Na metal intercalant (as the anode). Since the Na metal has a low electronegativity with a reduction potential of -2.714V, the Na-ions electrochemically intercalate into RGO interlayers and RGO-RGO sheet junctions along with the flowing current [45]. On the one hand, the intercalation of Na-ion can provide enough electrons (n-type doping) to shift up the Fermi level. When the storage amount of Na-ions in RGO interlayers is large enough, the accumulated electron doping is capable of causing the "Pauli blocking" [48] of visible incident light. The consequence is great enhancement of optical transmittance of RGO film. On the other hand, the junctions between RGO flakes serve as barriers for charge transport. Theoretically, reducing the influence of the junctions can improve the conductivity of the RGO film [26]. And it turns out that the Na-ion intercalation and the electron doping also make a contribution to the electron pathways and reduction of junction resistance. Figure 3-1(c) shows an AFM image of RGO film, which is very uniform and smooth on the nanoscale. The bright lines are overlapping and ripple of RGO flakes. Figure 3-1(d) shows a typical sample of Na-RGO film in air, which is highly transparent and air-stable [45].

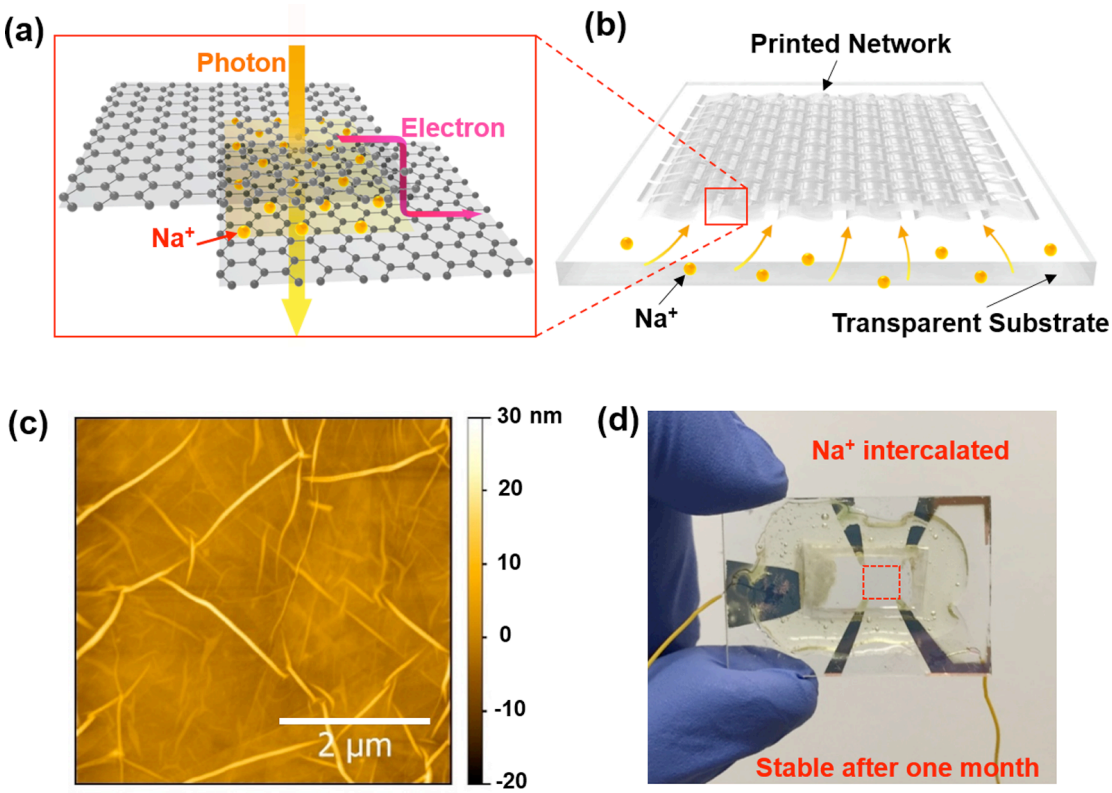

Figure 3-1. Na-ion intercalation process and RGO film. (a) Schematic of Na-ion intercalation between two RGO flakes. (b) Schematic of Na-ion intercalation in printed RGO film. (c) AFM image of printed RGO film. (d) High transparent and air-stable Na-RGO film. Figures adapted from ref. [45].

3.2 Material Characterizations

Figure 3-2(a) shows different layers of RGO films on glass substrate (1 to 6 layers from left to right). Figure 3-2(b) shows the Scanning Electron Microscopic (SEM) image of RGO on Si wafer; (Si wafer acting as conductive substrate for SEM). Figure 3-2(c) shows an optical microscope image of copper electrode deposited on RGO film.

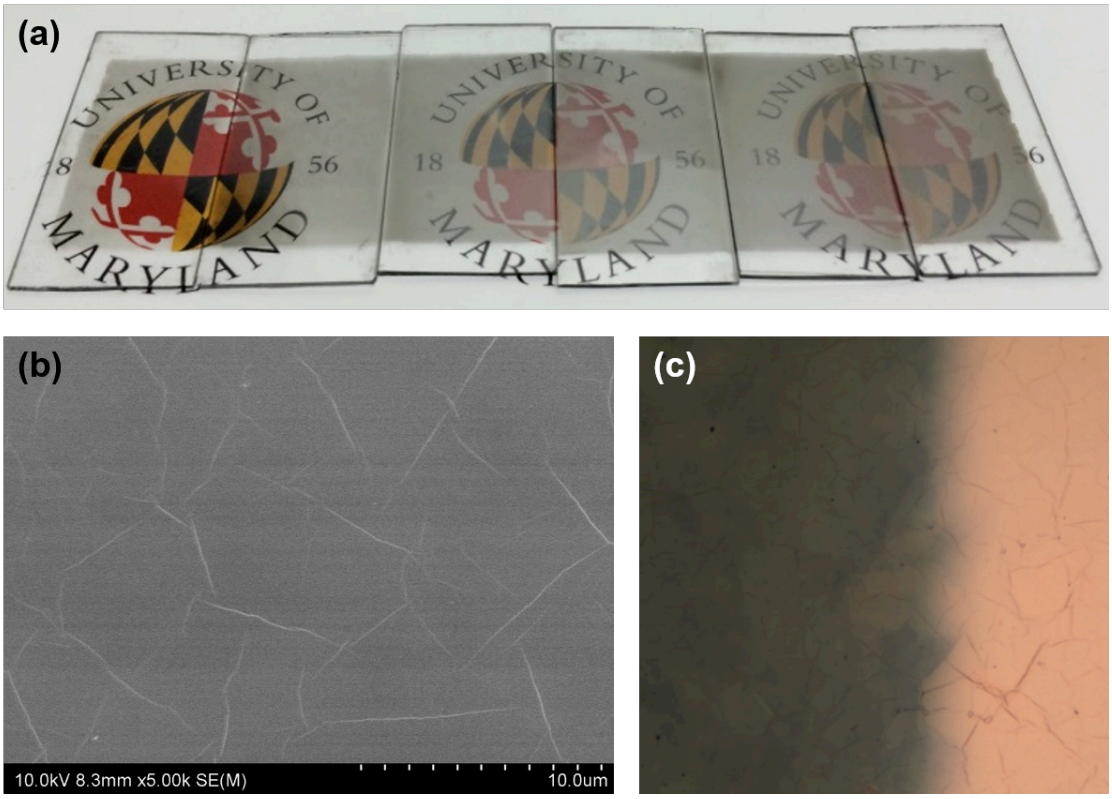

Figure 3-2. RGO films real images, SEM image and optical microscope image. (a) RGO film with different coating times from 1 to 6. (b) SEM image of RGO film. (c) Optical microscope image of copper electrode deposited on RGO film. Figures adapted from ref. [45].

Despite the principle of Na-ion intercalation, two material characterizations were also conducted in order to demonstrate Na-ions intercalation for the RGO is viable. To begin with, a coin-cell was fabricated with a freestanding RGO film as cathode and a piece of Na metal as anode. Then the cell was discharged and charged with the cycling voltammetry method. Figure 3-3(a) shows the voltage-capacity curve (second cycle) of RGO sodiation and desodiation at a small current density of 25 mA/g. From the data we can see that the sodiation process has a specific capacity of 170 mAh/g, and 127 mAh/g for desodiation [45]. The reversible specific capacity demonstrates successful Na-ions intercalation. The irreversible behavior is due to the formation of solid electrolyte interface, which is common for carbon-based anodes in Na-ion batteries [46]. From the reversible specific capacity we know that the amount of intercalated Na-ions in the RGO film is 0.028/carbon atom [45].

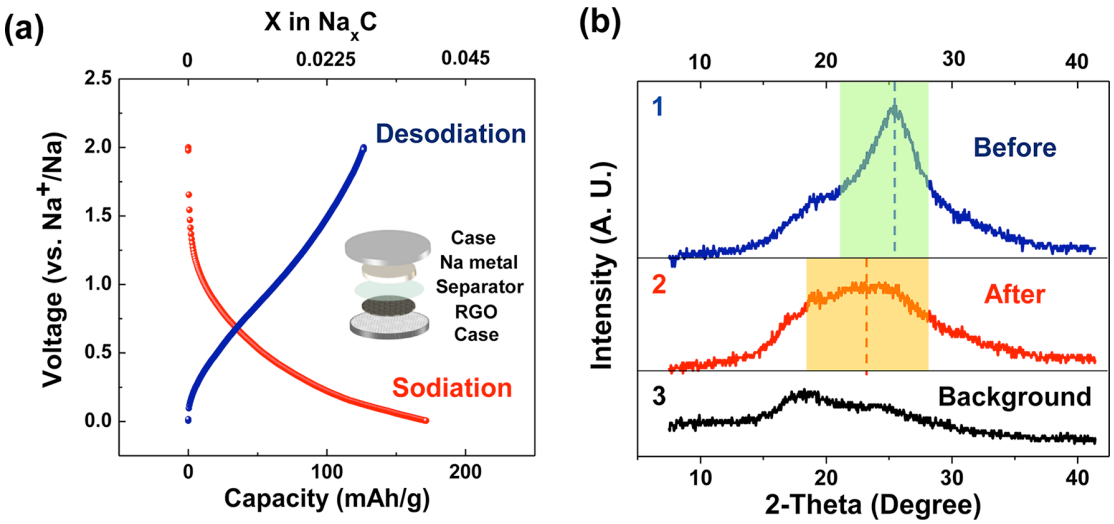

Figure 3-3. Voltage profile and X-Ray Diffraction of RGO film. (a) Voltage-capacity curve of RGO film as cathode in coin cell. Inset is the schematic of Na-RGO coin cell (b) XRD of RGO film before, after Na-ion intercalation, and background is plastic wrap. Figures adapted from ref. [45].

X-Ray Diffraction was also carried out with the same freestanding RGO film used in the coin cell before and after Na-ion intercalation. During the XRD testing, the RGO film was protected with a plastic wrap to avoid side-reaction with air under ambient condition. Figure 3-3(b) shows three peaks, blue peak, red peak and black peak. The black peak is at the position of 18°, corresponding to the plastic wrap background. The blue peak at the position of 25.35° represents the RGO film before Na-ions intercalation. This peak position represents the interlayer distance of RGO around 3.49 Å, which is larger than the interlayer distance of pristine graphite (3.35 Å). The green shadow range corresponds to the peak with full width at maximum (FWHM), which has a length of 1.02 Å [45]. The position of the red peak corresponds to the Na-RGO film, which indicates that the peak shifted to the left after Na-ions intercalation. This peak position shows that the interlayer distance of Na-RGO is around 3.76 Å, which is larger than the interlayer distance of RGO (3.49 Å). Yellow shadow range corresponds to the peak with full width at maximum (FWHM) in length of 1.67 Å. The larger interlayer distance of Na-RGO demonstrates a successful Na-ions intercalation between RGO layers and flakes [45].

3.3 Optical and Electrical Properties

3.3.1 Optical Transmittance

The images of Figure 3-4(a) show the real images and optical microscope images before and after Na-ion intercalation, RGO film became much more transparent after Na-ion intercalation. The transmittance of Na-ion intercalated RGO

(Na-RGO) clearly increased a lot after Na-ion intercalation. The transmittance of the RGO film before and after Na-ion intercalation is quantitatively calculated by grey part of the images captured by an optical microscope (transmission mode) respectively, as shown in Figure 3-3(a). The increase in optical transmittance was uniform for the whole RGO film. Figure 3-4(b) plots the transmittance change of RGO film before and after complete Na-ion intercalation at 550 nm wavelengths for samples with different thickness [45]. It is obvious to see that all samples had a drastic transmittance enhancement when the glass substrate was excluded in the transmittance measurement. Wavelength dependent spectrum from 450 nm to 900 nm is shown in Figure 3-4(c). The optical transmittance vs. wavelength of Na-RGO in the visible range indicates a neutral color, which is useful for practical applications.

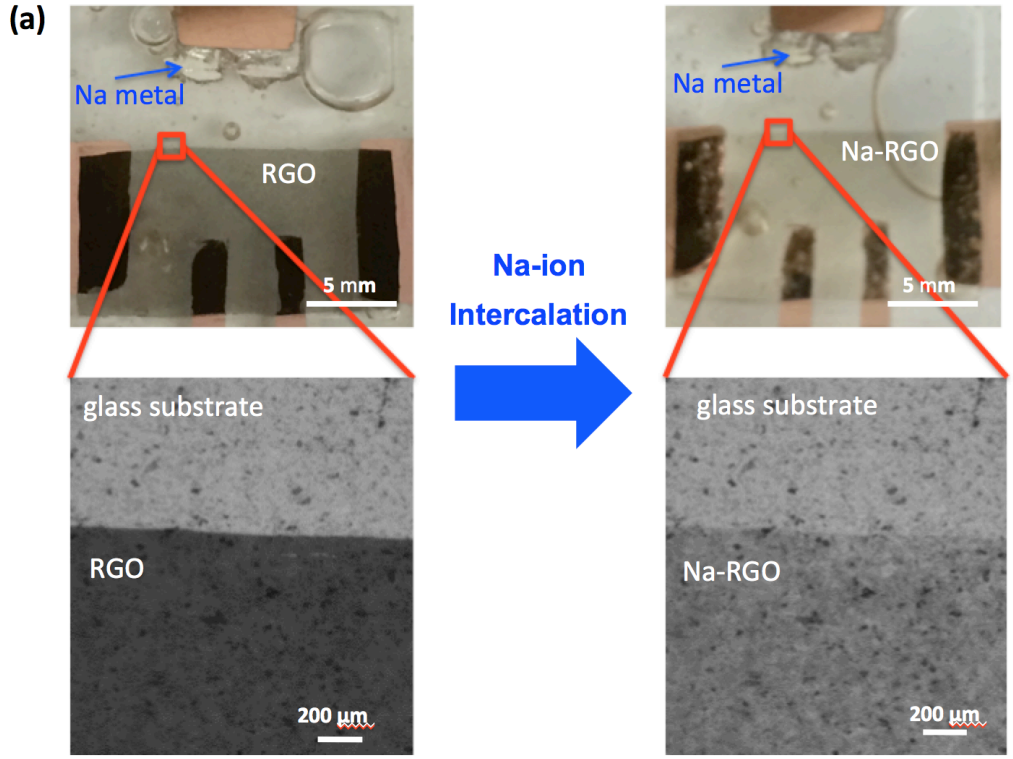

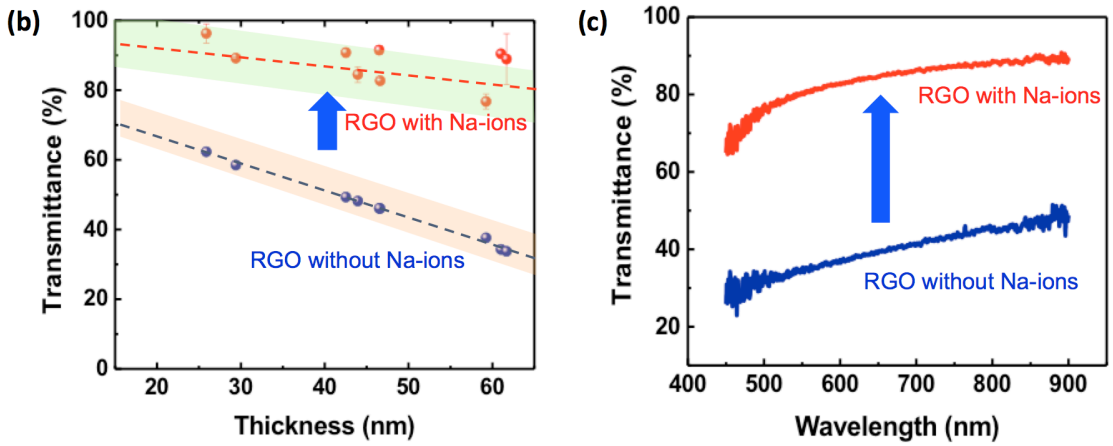

Figure 3-4. Transmittance of RGO films before and after Na-ion intercalation. (a) Real images and optical microscope images of a RGO film before and after Na-ion intercalation. (b) Transmittance at 550 nm vs. thickness of RGO film before and after Na-ion intercalation at 550 nm. (c) Transmittance vs. wavelength of a RGO film before and after Na-ion intercalation with a visible spectrum from 450 nm to 900 nm. Figures adapted from ref. [45].

3.3.2 Electrical Conductivity

Besides optical transmittance, the other critical property for TCFs is electrical conductivity, which is evaluated by the sheet resistance. Therefore, the sheet resistance of RGO film before and after Na-ion intercalation was also studied in details. Sheet resistance was measured by four-probe method as shown in insets of Figure 3-5(a). First, four copper electrodes were deposited on top of RGO, where the RGO film is 5 mm x 10 mm. And the distance between two copper electrodes in the center is 5 mm. So, the RGO film in the center is 5 mm x 5 mm. Four copper electrodes were designed in this way to eliminate the contact resistance between copper electrodes and RGO film and to facilitate the measurement. Figure 3-5(a)

shows the I-V curve of a RGO film before and after Na-ion intercalation. Before Na-ion intercalation, the sheet resistance was around 100 kΩ/sq, due to the incomplete reduction of the GO film at 300 °C. After Na-ion intercalation, the sheet resistance decreased dramatically as shown from the relatively small slope. Figure 3-5(b) shows sheet resistance changes of two typical samples. After Na-ion intercalation, the sheet resistance decreased from 523 kΩ/sq to 1467 Ω/sq and from 83 kΩ/sq to 311 Ω/sq, which are around 300 times decreasing [45]. This can be explained by the enhancement of carrier density caused by Na-ion doping for RGO, which results in conductivity increasing [47]. Additionally, Na-ion intercalation has the potential to enhance the contact between RGO flakes and improve the junction resistance, which is a common issue in film transparent conductive electrode [49].

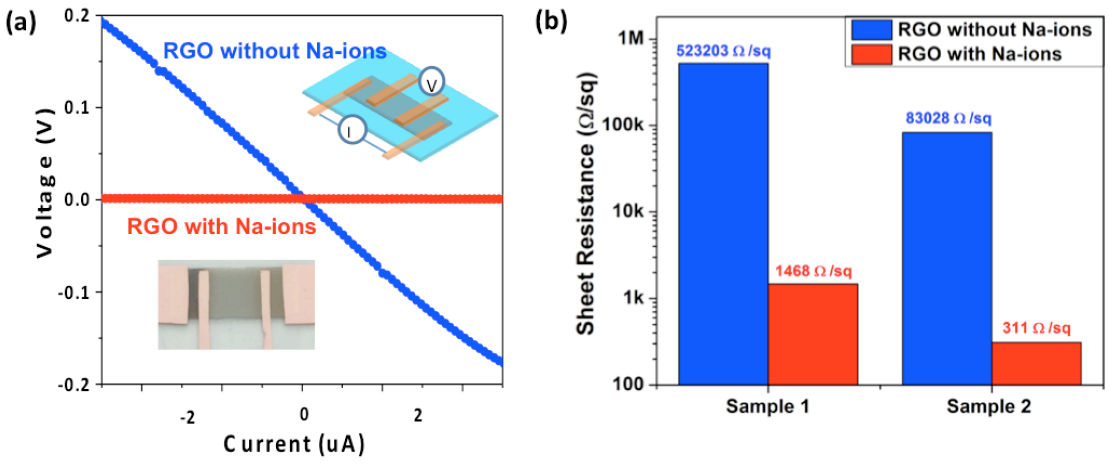

Figure 3-5. Sheet resistance of RGO film before and after Na-ion intercalation. (a) I-V curve of four-probe measurement of a RGO film before and after Na-ion intercalation. Insets are the schematic and real images of four-probe measurement. (b) Sheet resistance of two samples before and after Na-ion intercalation. Figures adapted from ref. [45].

3.3.3 Figure of Merit

From above two sectors we can see, there is a simultaneous enhancement of optical transmittance and conductivity (decrease of sheet resistance) after Na-ion intercalation. This is mainly due to the electron doping provided by intercalated Na-ions, and the Na-ion doped RGO films. Large amount of electron doping resulted in a Fermi level upshift and blocks optical transition in visible light wavelength, therefore caused the optical transmittance increase [45]. Also, the intercalated Na-ions provide better contact between RGO flakes and junctions, which lowered the sheet resistance.

Compare our work with other RGO-based transparent conductive electrode or film, as shown in Figure 3-6(a), Na-RGO film has the best-combined performance of them. As the standard discussed in Chapter 1, the Figure 3-6(b) shows the figure of merit (FOM, the ratio of electrical conductivity over optical conductivity, $\frac{\sigma_{DC}}{\sigma_{OP}}$) is used based on sheet resistance and optical transmittance at 550 nm. Compared to other reported RGO-based transparent conductors, Na-RGO film gives the highest FOM value [45].

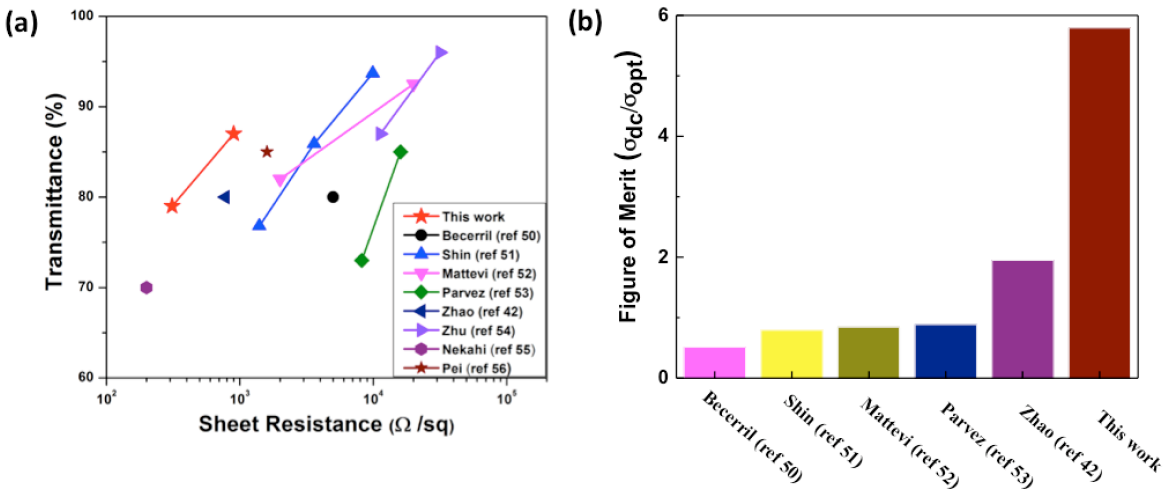

Figure 3-6. Comparison between Na-RGO films from this work and previous reported RGO-based films. (a) Transmittance at 550 nm vs. Sheet Resistance of Na-RGO film and other RGO transparent conductors. (b) FOM of RGO-based transparent electrodes. Figures adapted from ref. [45].

3.3.4 Controllability of Na-ion Intercalation

The controllability of the doping is an important issue in the electrode application by changing conditions of electrochemical intercalation. As demonstrated in material characterization part, a coin cell is tested and showed a reversible sodiation/desodiation process of a RGO freestanding film. Similar to the coin cell, the Na-RGO planar-battery is actually a battery. From Li-ion intercalated few-layer graphene we know, Li doping in few-layer graphene was controlled at different plateau regions. At the end of different plateau at 0.2V, 0.1V and 0.05V, the lithiated compound is well known as LiC_{36}, LiC_{12}, and LiC_6, respectively [40]. Unlike the Li intercalation in few-layer graphene case, no plateau in Na-RGO voltage profile is observed. Therefore, the Na-ion intercalation was manually controlled at different cut-off voltage with a battery tester, and *in situ* measured the resistance change of the film. Figure 3-7(a) shows real images of RGO film with different cut-off voltages during Na-ion intercalation process. In Figure 3-7(b), planar battery was kept at each voltage for 30 minutes, with cut-off voltage of 1V, 0.5V, 0.4V, 0.3V, 0.2V, 0.1V, and 0V. The resistance of original RGO film was 43.8 kΩ before Na-ion intercaltion. Figure 3-7(c) clearly shows the resistance of RGO film during sodiation process at different cut-off voltages. After the voltage reached 0 V (vs. Na/Na+) and kept for

half an hour, the resistance is 2.09 kΩ. Then the 0 V (vs. Na/Na+) was kept for another 11 hours, the resistance dropped to 900 Ω. In summary, a trend of decreasing resistance with decreasing cut-off voltage was demonstrated through *in situ* measurement of Na-RGO planar battery, which proves the controllability of Na-ion intercalation in RGO.

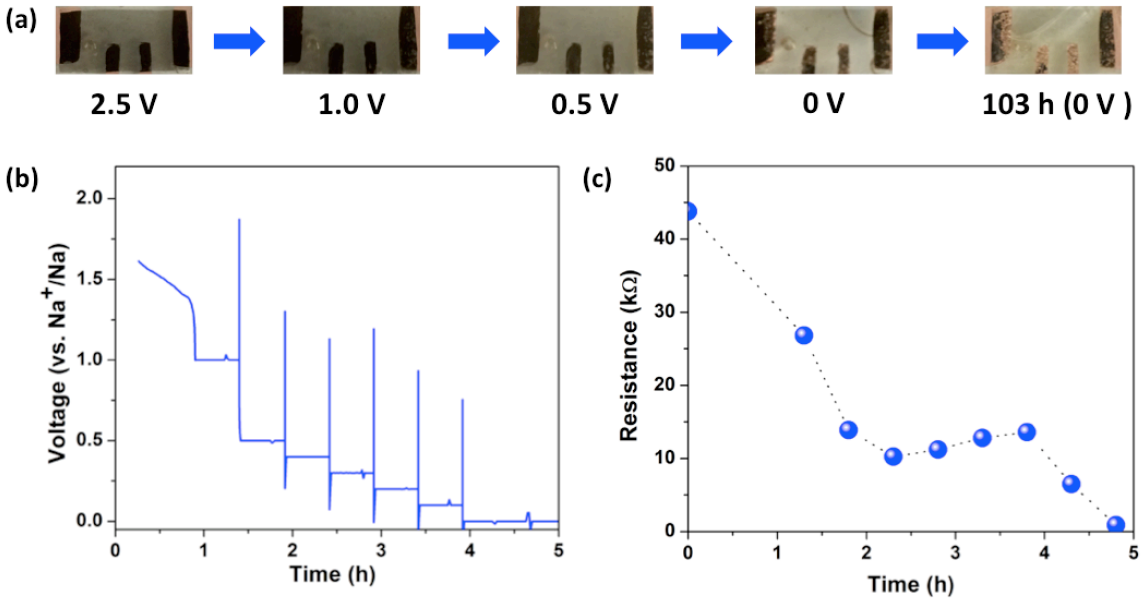

Figure 3-7. *In situ* measurement of resistance of Na-RGO film with planar battery. (a) Real images of RGO film with different cut-off voltages during Na-ion intercalation. (b) Voltage profile of planar battery at different cut-off voltages. (c) Resistance of RGO film during Na-ion intercalation at different cut-off voltages.

3.3.5 Air Stability of Na-RGO Films

The RGO planar battery device is liquid-based electrochemical system, which has high active Na metal as anode. Therefore, the stability of Na-RGO film should be evaluated as well. The planar battery was disassembled to expose the Na-RGO in air (ambient surrounding) after complete Na-ion intercalation. Optical microscope

images were taken on the same position of two Na-RGO film samples respectively after air exposure for 0, 0.5, 2, 3 and 13 hours [45]. Figure 3-8(a) shows the transmittance change of two Na-RGO film samples before and after exposure in air. For sample 1 (red bar), the transmittance of RGO film enhanced from 57% to 90% after Na-ion intercalation. After exposed in air, the transmittance decreased a little bit over time and stabled at around 80% after 13 hours. One month later, the transmittance still did not change very much. Figure 3-8(b) shows the real images of sample 1 [45].

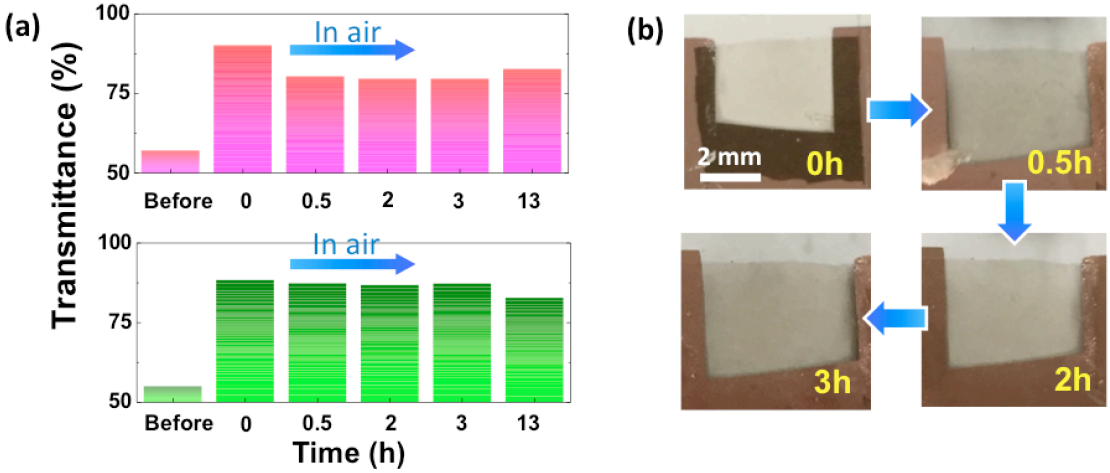

Figure 3-8. Transmittance air-stability of Na-RGO film. (a) Transmittance change of two Na-RGO film samples before and after exposure in air. (b) Real images of Na-RGO in air after 0, 0.5, 2 and 3 hours. Figures adapted from ref. [45].

For the Li-ions intercalated few-layer graphene, the graphene becomes very transparent after Li-ion intercalation. But the intercalated LiC_6 composite would change back to the pristine transmittance after a few hours in air due to the poor stability of Li-ions [40]. The stability of Na-ion intercalated RGO film can be

explained as following. The alkaline metal or ions (here is Na-ions) are active and could react with oxygen and water in ambient air surroundings. Comparing with Li-ions, Na-ions have larger size and lower diffusivity through the barriers. The reactants on edges of 2D materials such as RGO prevent the reactions with H_2O, O_2 and CO_2 in air, and trapped intercalated Na-ions inside the RGO interlayers and flakes [45].

Figure 3-9 describes the transmittance change before and after Na-ion intercalation of a RGO film sample, and long-term transmittance change of this Na-RGO film after air exposure. The optical transmittance of RGO film is 62.0% before intercalation. After it fully become to Na-RGO, the transmittance enhanced to 91.2%. Disassemble the device and expose the Na-RGO film in air, and after 6 hours, the transmittance decreased to 80.7%. The transmittance of the Na-RGO film was further tested up to 9 days. Start from day 4 (96 hours), the optical transmittance remains a constant value of 77%. These data prove the long-term stability of optical transmittance.

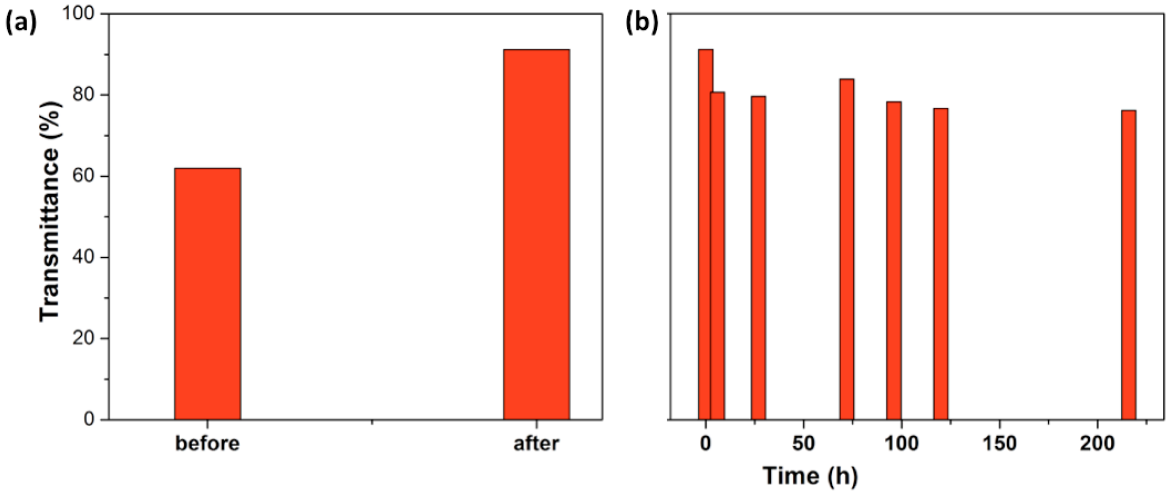

Figure 3-9. Transmittance (a) before and after Na-ion intercalation, and (b) transmittance change after air exposure.

Similar to the air stability of transmittance of Na-RGO film, the air-stability of resistance is also vital for practical application of transparent conductor. However, the stability of resistance is more difficult to measure, which involves thin Cu electrodes (50 nm). When electrolyte dries out, the contact between Cu electrodes and RGO film is easy to break making it hard to test the resistance stability. Therefore, the resistance stability of the Na-RGO film was tested while keep soaking the Na-RGO film in electrolyte (open circuit). Real images of the device are shown in Figure 3-10(a). The resistance of Na-RGO film was kept at 0V (vs. Na/Na+) for 11 hours and the resistance reached 900 Ω. Then, disconnect the Na metal and Na-RGO electrodes. After 4 days, the resistance only increased to 984 Ω, which demonstrated the resistance stability of Na-RGO film (Figure 3-10(b)).

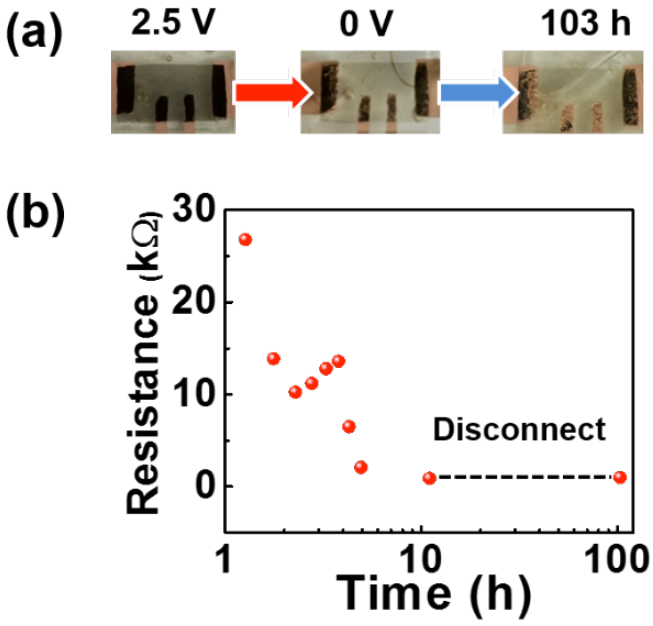

Figure 3-10. Resistance change of Na-ion intercalated RGO during and after Na-ion intercalation. (a) Real images of RGO film, Na-RGO film, and air-exposed Na-RGO film for 4 days. (b) Resistance during Na-ion intercalation (for 11 hours), and resistance change of air-exposed and disconnected Na-RGO (for 4 days).

3.4 Further Enhancement

3.4.1 Surfactant-free RGO Film Fabrication Method

The GO ink used for Meyer rod coating was added surfactant Zonyl to reduce the surface tension, which might have an influence on the degree of GO reduction. Therefore, a surfactant-free method has been carried out to take care of this issue. By adding same amount of ethanol to replace surfactant, a uniform coating of GO is achieved, as shown in Figure 3-11(a). GO can also be printed uniformly on glass slide with this surfactant free method. And after thermal reduction under the same conditions, the RGO film is still uniform as shown in Figure 3-11(b).

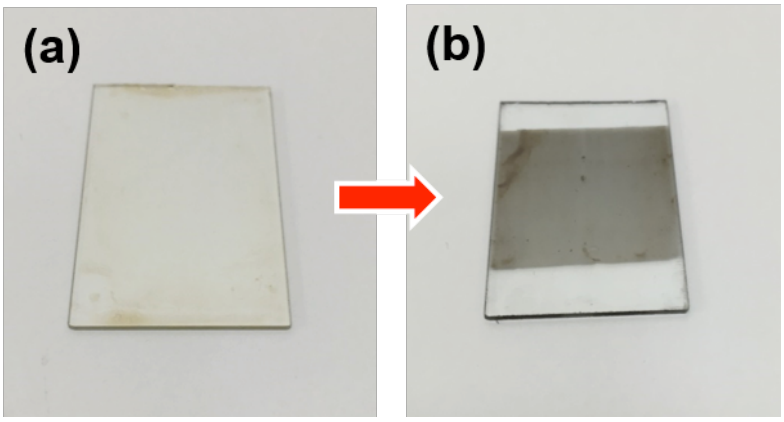

Figure 3-11. Surfactant-free GO film and RGO film, respectively. (a) Uniform GO film and (b) RGO film before and after thermal reduction by surfactant-free method.

X-Ray Diffraction (XRD) is used to characterize the reduction degree in RGO film by analyzing its interlayer distance. Figure 3-12 shows the XRD result of GO film and RGO film. The peak positions for these films are at 10.2° and 25.3°, corresponding to interlayer distances of 8.70 Å and 3.49 Å. Comparing to the interlayer distance of graphite at 3.35 Å, the RGO reduced at 300 °C is not completely recovered to graphite. The larger interlayer distance compares to graphite enables the Na ion intercalation in between the RGO layers.

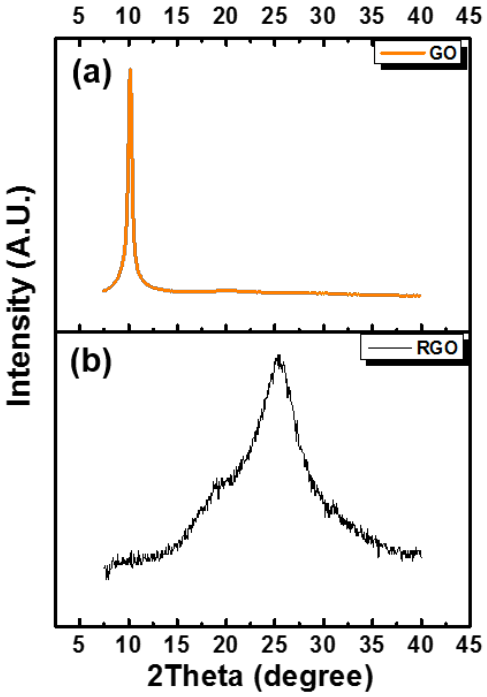

Figure 3-12. XRD before (a) and after (b) thermal reduction of GO film at 300 °C.

3.4.2 Hydroiodic Acid Reduced Na-RGO Film Fabrication

The thermal reduction annealing method for RGO requires high reduction temperature (300 °C), the method might not be applicable on flexible substrates. Therefore, chemical reduction with hydrazine was also tried owing to its low

temperature and solution based reduction conditions, which might be useful for applications such as flexible electronics. HI was used as a chemical reductant to reduce GO, and the result is show in figure above. Figure 3-13(a) shows GO coated glass substrate, and (b) shows HI solution in 60 °C water bath. After 15 seconds of immerse, GO were reduced with similar optical transmittance as the thermal reduced samples. Figure 3-13(d,e) show the microscope images of HI reduced GO before and after Na-ion intercalation. The Na-ion intercalation also greatly enhanced the transmittance of RGO film (from 44% to 96%), suggesting that it is a universal approach for enhancing the performance of RGO film as transparent electrodes.

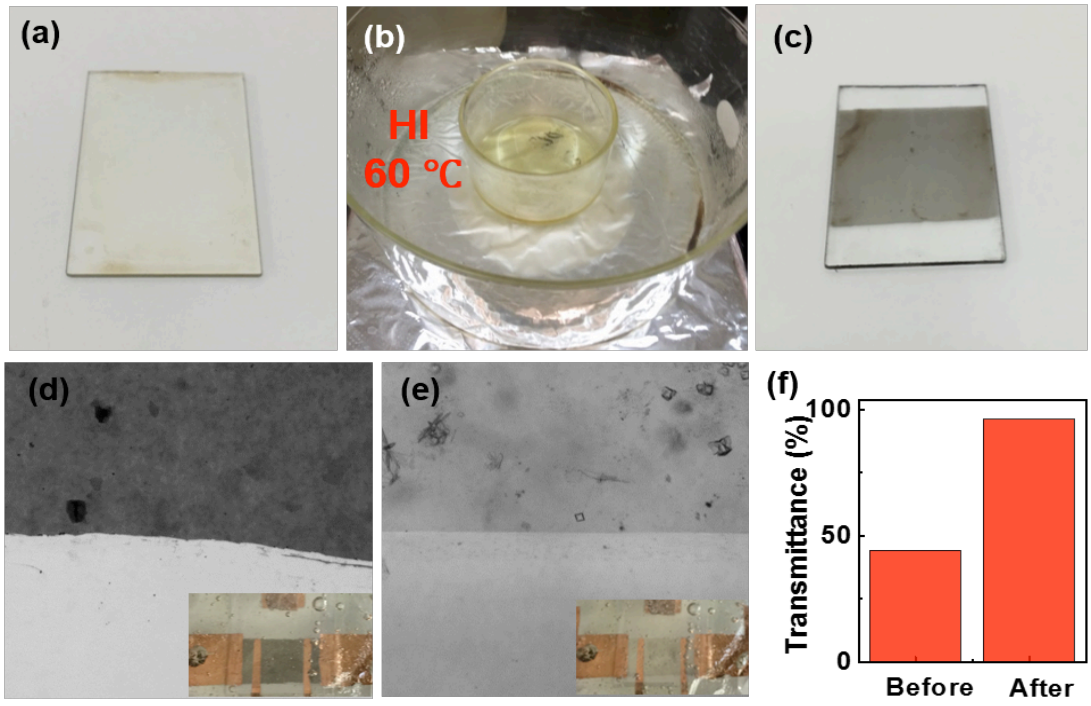

Figure 3-13. RGO Film Fabrication and Properties with HI Reduction Method. (a) GO coated glass substrate (surfactant free ink). (b) HI reduction set up, HI solution in 60 °C water bath. (c) GO film after 15 seconds of HI reduction. (d-e) microscope image of HI reduced RGO before and after Na-ion intercalation, inset are real images

of HI reduced RGO before and after Na-ion intercalation. (f) Transmittance change before and after Na-ion intercalation.

3.4.3 Na-RGO Film with Large Area RGO Flakes

Graphene oxide (GO) ink used in previous experiments of this work was prepared from ~150 μm natural graphite flakes (Sigma-Aldrich, cat #332461). As Zhao [42] reported that, the size of the graphite flakes may have an influence on the size of the graphene oxide sheets. Ideally, larger graphene oxide sheets would have fewer junctions and contacts, which could potentially lower the sheet resistance. Therefore, ~500 μm natural graphite flakes (Asbury Carbons) was used to prepare graphene oxide and fabricate RGO films for performance improvement purpose. Figure 3-14(a,b) shows the real images and microscope images comparisons of ~150 μm and ~500 μm natural graphite flakes. The latter obviously has larger graphite flakes than those used in previous experiments.

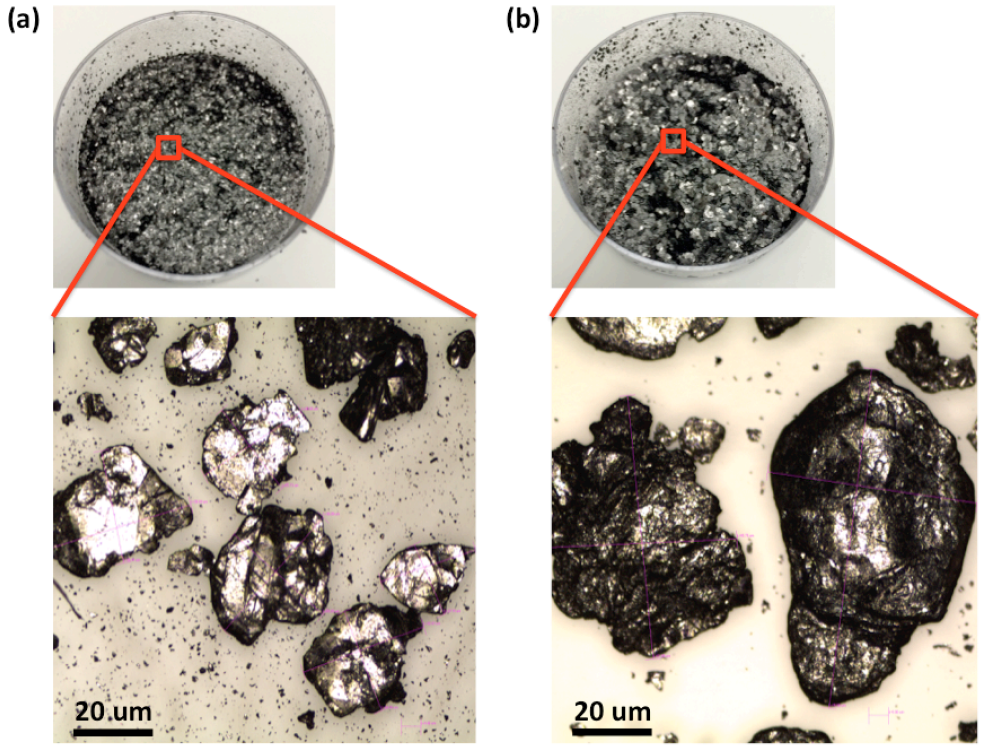

Figure 3-14. Real images and optical microscope images of (a) ~150 μm natural graphite flakes (Sigma-Aldrich) and (b) ~500 μm natural graphite flakes (Asbury Carbons).

Figure 3-15(a) shows typical optical microscope image of GO sheets prepared from~150 μm graphite flakes and ~500 μm graphite flakes obtained by modified Hummer`s method, respectively. The respective area distributions in Figure 3-15(c,d) are on the basis of Microscope measurements on 250 sheets for each batch of GO. It is seen that about 70% of the GO sheets prepared from~150 μm graphite flakes are less than 500 μm^2 (Figure 3-15(c)). Nevertheless, only about 35% of the GO sheets prepared from~500 μm graphite flakes are less than 500 μm^2. And about 50% of area

of the GO sheets prepared from ~500 μm graphite flakes are 500-5000 μm^2, whose average area is much larger than former GO sheets (Figure 3-15(d)).

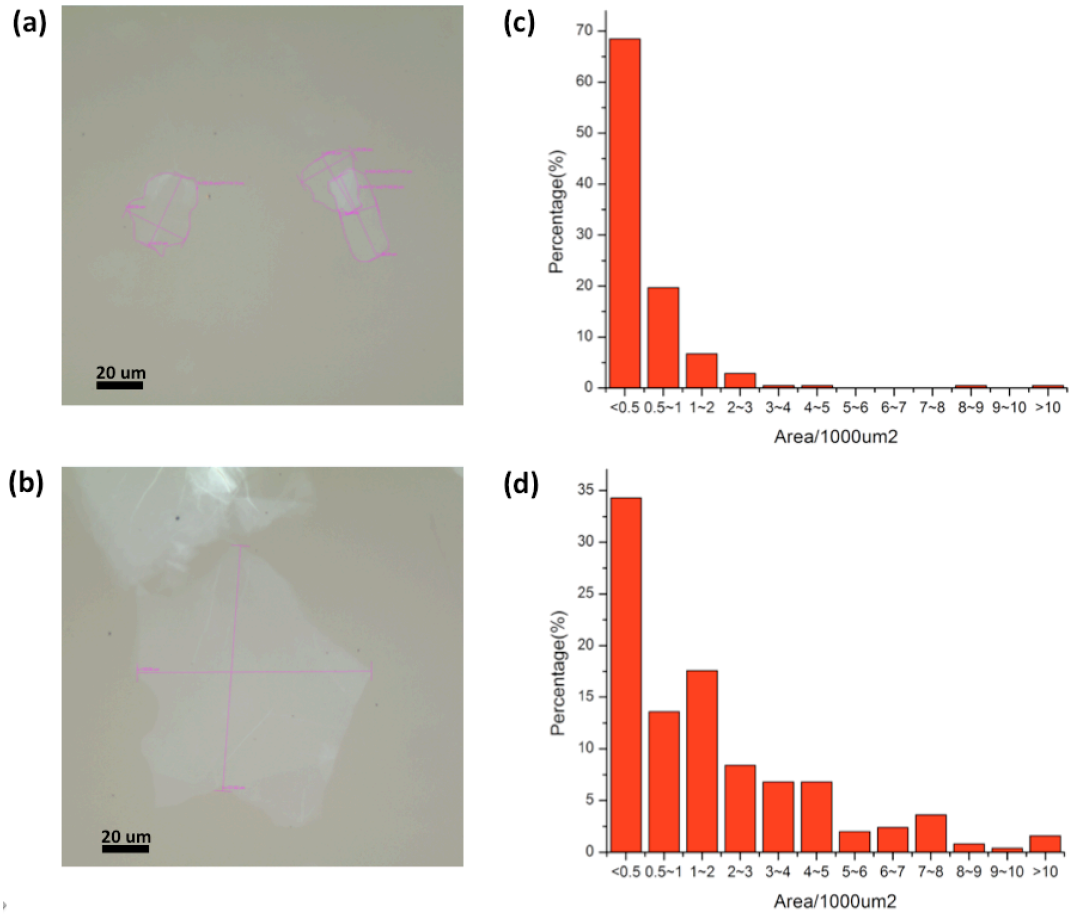

Figure 3-15. Optical microscope images and area distributions of GO sheets prepared from ~150 μm (a,c) and ~500 μm graphite flakes (b,d), respectively.

As shown in Figure 3-16, the typical transmittance of RGO film (prepared from 500 μm graphite flakes) changed from less than 40% to over 80% before and after Na-ion intercalation. The sheet resistance before Na-ion intercalation is 2.29 kΩ/sq, which is much smaller than RGO film prepared from 150 μm graphite flakes (around

100 kΩ/sq). This can be explained by the larger average RGO flakes provide fewer RGO-RGO junctions and contacts between flakes. After Na-ion intercalation, the sheet resistance is 29.14 kΩ/sq. Though the sheet resistance becomes larger, this method still shows great potential of enhancement in both transmittance and sheet resistance. Further optimization experiments need to be carried out to achieve conductivity enhancement.

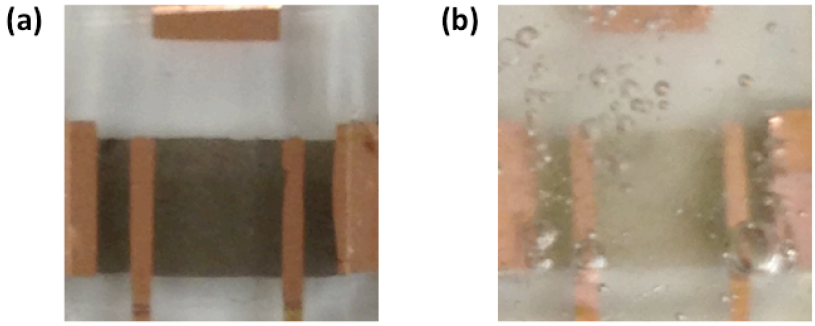

Figure 3-16. Real images of RGO film (prepared from 500 μm graphite flakes) before (a) and after (b) Na-ion intercalation.

Chapter 4: Summary and Future Work

4.1 Summary

This work has shown great that the optical transmittance and electrical conductivity of RGO films could be enhanced simultaneously through the process of Na-ion intercalation. The Na-RGO films have shown excellent performance, comparing with other RGO-based transparent conductors in previous reported publications. The work has achieved large-scale TCFs at low-cost with a Meyer-rod printing method. The general fabrication processes for TCFs are scalable towards practical applications, including GO film printing, thermal reduction/ chemical reduction and electrochemical intercalation process. Comparing with Li-ion intercalated few-layer graphene, Na-RGO films also have shown great air stability for practical applications, optically and electrically.

4.2 Future Work

This work has shown great potential of metal ion intercalations for practical transparent conductive film applications. Future work includes RGO films with large-scale RGO flakes, mechanical toughness of Na-RGO films during Na-ion intercalation and tunable work function study of Na-RGO films. This work has shown great potential of metal ion intercalations for practical transparent conductive film applications.

As shown in Chapter 3, the RGO films prepared by larger RGO flakes have a significantly lower initial sheet resistance at 2.29 kΩ/sq (compared with 100 kΩ/sq made with previous GO ink). The problem for this method is that the contact between copper electrodes and RGO film becomes worse after Na-ion intercalation. Therefore, the sheet resistance was much larger after Na-ion intercalation. A possible solution is to thermally reduce the RGO film at a low temperature to strengthen the overlapping area after the copper electrode deposition.

The chemical reduction method has proven to be an effective fabrication method, compared with the time-consuming and costly thermal reduction process. However, during and after Na-ion intercalation for RGO films, there will be peeling off areas on Na-RGO films and bubbles on overlapping areas between Copper electrode and RGO film. The reason is due to the weak mechanical strength of HI reduced RGO film, which contains liquid acid solution inside the RGO-RGO flakes. After Na-ion intercalation, the intercalated Na-ions in RGO film may introduce tensile strength, which could cause expansion in the local RGO domain. This problem could be improved by an additional thermal reduction step at low temperature (150°C) after the HI chemical reduction process. Another viable method is to print a polymer layer on top of RGO film for fixation during Na-ion intercalation. These methods could enhance the mechanical strength of Na-RGO films.

The work function is also an important parameter that could influence the properties of TCFs. Work function of TCFs is the minimum energy required to remove an electron from conduction band. The measurement methods for work

function, such as UPS measurement and kelvin probe measurement, require an exposure of Na-RGO film into air. And the Na-ion intercalation is an electrochemical process, which involves liquid electrolyte. After disassembling the RGO device, a layer of $NaPF_6$ salt will stay on the Na-RGO surface when the electrolyte dries out. This $NaPF_6$ layer hinders either UPS or kelvin probe measurement. Even if the whole device is immersed in pure EC/DEC solution for 30 mins, the $NaPF_6$ salt still stays on top of the Na-RGO film. Therefore, there is difficulty in measuring the work function and Fermi level directly through the Na-RGO films for current electrochemical platform system. *Kumar* [57] reported a method to tune the work function of RGO by changing the concentration of oxygen function groups (epoxy and carbonyl groups) and achieved a 2.5 eV change. In order to change the concentration of oxygen function groups, the thermal reduction temperature could be increased to over 450° C (The temperature used in this study is 300 ° C). Thermal reduction temperature has an influence on the degree of reduction and C/O ratio [58].

Reference

[1] Ellmer, Klaus. "Past achievements and future challenges in the development of optically transparent electrodes." *Nature Photonics* 6.12 (2012): 809-817.

[2] Wang, Xuan, Linjie Zhi, and Klaus Müllen. "Transparent, conductive graphene electrodes for dye-sensitized solar cells." *Nano letters* 8.1 (2008): 323-327.

[3] Yang, Yajie, et al. "Ordered and ultrathin reduced graphene oxide LB films as hole injection layers for organic light-emitting diode." *Nanoscale research letters*9.1 (2014): 1-6.

[4] Bae, Sukang, et al. "Roll-to-roll production of 30-inch graphene films for transparent electrodes." *Nature nanotechnology* 5.8 (2010): 574-578.

[5] Yu, K.; Chen, J. *Materials Matters* 2014, 9, (1), 6-13

[6] Seeger, K. *Semiconductor Physics* Ch 4 (Springer, 1991)

[7] Gordon, Roy G. "Criteria for choosing transparent conductors." *MRS bulletin*25.08 (2000): 52-57.

[8] Pankove, J. I. *Optical Processes in Semiconductors* Ch 1 (Dover, 1971).

[9] Kittel, Charles, Paul McEuen, and Paul McEuen. *Introduction to solid state physics*. Vol. 8. New York: Wiley, 1976.

[10] Dressel M and Gruner G 2002 Electrodynamics of Solids:Optical Properties of Electrons in Matter (Cambridge:Cambridge University Press)

[11] Minami, Tadatsugu. "Transparent conducting oxide semiconductors for transparent electrodes." *Semiconductor Science and Technology* 20.4 (2005): S35.

[12] Lampert, Carl M. "Heat mirror coatings for energy conserving windows." *Solar Energy Materials* 6.1 (1981): 1-41.

[13] Ginley, D. S., Hosono, H. & Paine, D. C. *Handbook of Transparent Conductors* (Springer, 2010).

[14] Ishibashi, S., et al. "Low resistivity indium–tin oxide transparent conductive films. II. Effect of sputtering voltage on electrical property of films." *Journal of Vacuum Science & Technology A* 8.3 (1990): 1403-1406.

[15] Betz, Ulrich, et al. "Thin films engineering of indium tin oxide: large area flat panel displays application." *Surface and Coatings Technology* 200.20 (2006): 5751-5759.

[16] Chopra, K. L., S. Major, and D. K. Pandya. "Transparent conductors—a status review." *Thin solid films* 102.1 (1983): 1-46.

[17] Furubayashi, Y. *et al.* A transparent metal: Nb-doped anatase TiO2. *Appl. Phys. Lett.* 86, 252101 (2005)

[18] Hu, Liangbing, et al. "Scalable coating and properties of transparent, flexible, silver nanowire electrodes." *ACS nano* 4.5 (2010): 2955-2963.

[19] Sepulveda-Mora, Sergio B., and Sylvain G. Cloutier. "Figures of merit for high-performance transparent electrodes using dip-coated silver nanowire networks."*Journal of Nanomaterials* 2012 (2012): 9.

[20] Spotnitz, Matthew E., Declan Ryan, and Howard A. Stone. "Dip coating for the alignment of carbon nanotubes on curved surfaces." *Journal of Materials Chemistry* 14.8 (2004): 1299-1302.

[21] Hu, L., D. S. Hecht, and G. Grüner. "Percolation in transparent and conducting carbon nanotube networks." *Nano Letters* 4.12 (2004): 2513-2517.

[22] Rathmell, Aaron R., et al. "The growth mechanism of copper nanowires and their properties in flexible, transparent conducting films." *Advanced materials*22.32 (2010): 3558-3563.

[23] Sreekumar, T. V., et al. "Single-wall carbon nanotube films." *Chemistry of Materials* 15.1 (2003): 175-178.

[24] Manivannan, S., et al. "Properties of surface treated transparent conducting single walled carbon nanotube films." *Journal of Materials Science: Materials in Electronics* 21.1 (2010): 72-77.

[25] Dan, Budhadipta, Glen C. Irvin, and Matteo Pasquali. "Continuous and scalable fabrication of transparent conducting carbon nanotube films." *ACS nano* 3.4 (2009): 835-843.

[26] Star, Alexander, et al. "Preparation and properties of polymer−wrapped single−walled carbon nanotubes." *Angewandte Chemie International Edition*40.9 (2001): 1721-1725.

[27] Niu, Chunming. "Carbon nanotube transparent conducting films." *MRS bulletin*36.10 (2011): 766-773.

[28] ("This Month in Physics History: October 22, 2004: Discovery of Graphene". APS News. Series II 18 (9): 2. 2009.)

[29] Lee, Changgu, et al. "Measurement of the elastic properties and intrinsic strength of monolayer graphene." *science* 321.5887 (2008): 385-388.

[30] Kuzmenko, A. B., et al. "Universal optical conductance of graphite." Physical review letters 100.11 (2008): 117401.

[31] Balandin, Alexander A. "Thermal properties of graphene and nanostructured carbon materials." *Nature materials* 10.8 (2011): 569-581.

[32] Geim, Andre K., and Konstantin S. Novoselov. "The rise of graphene." Nature materials 6.3 (2007): 183-191.

[33] Moser, Joel, Amelia Barreiro, and Adrian Bachtold. "Current-induced cleaning of graphene." *Applied Physics Letters* 91.16 (2007): 163513.

[34] Loh, Kian Ping, et al. "The chemistry of graphene." *Journal of Materials Chemistry* 20.12 (2010): 2277-2289.

[35] Bonaccorso, Francesco, et al. "Graphene photonics and optoelectronics."*Nature photonics* 4.9 (2010): 611-622.

[36] Becerril, Héctor A., et al. "Evaluation of solution-processed reduced graphene oxide films as transparent conductors." *ACS nano* 2.3 (2008): 463-470.

[37] Eda, Goki, Giovanni Fanchini, and Manish Chhowalla. "Large-area ultrathin films of reduced graphene oxide as a transparent and flexible electronic material." *Nature nanotechnology* 3.5 (2008): 270-274.

[38] Obraztsov, Alexander N. "Chemical vapour deposition: making graphene on a large scale." *Nature nanotechnology* 4.4 (2009): 212-213.

[39] Khrapach, Ivan, et al. "Novel Highly Conductive and Transparent Graphene−Based Conductors." Advanced Materials 24.21 (2012): 2844-2849.

[40] Bao, Wenzhong, et al. "Approaching the limits of transparency and conductivity in graphitic materials through lithium intercalation." Nature communications 5 (2014).

[41] Kaiser, Alan B. "Electronic transport properties of conducting polymers and carbon nanotubes." *Reports on Progress in Physics* 64.1 (2001): 1.

[42] Zhao, Jinping, et al. "Efficient preparation of large-area graphene oxide sheets for transparent conductive films." *Acs Nano* 4.9 (2010): 5245-5252.

[43] Hwang, Jin Ok, et al. "Workfunction-tunable, N-doped reduced graphene transparent electrodes for high-performance polymer light-emitting diodes." *Acs Nano* 6.1 (2011): 159-167.

[44] Khrapach, Ivan, et al. "Novel Highly Conductive and Transparent Graphene−Based Conductors." *Advanced Materials* 24.21 (2012): 2844-2849.

[45] Wan, Jiayu, et al. "Sodium-Ion Intercalated Transparent Conductors with Printed Reduced Graphene Oxide Networks." *Nano letters* (2015).

[46] Wen, Yang, et al. "Expanded graphite as superior anode for sodium-ion batteries." *Nature communications* 5 (2014).

[47] Marcano, Daniela C., et al. "Improved synthesis of graphene oxide." *ACS nano*4.8 (2010): 4806-4814.

[48] Mak, Kin Fai, et al. "Optical spectroscopy of graphene: from the far infrared to the ultraviolet." *Solid State Communications* 152.15 (2012): 1341-1349.

[49] Hecht, David S., Liangbing Hu, and Glen Irvin. "Emerging transparent electrodes based on thin films of carbon nanotubes, graphene, and metallic nanostructures." *Advanced Materials* 23.13 (2011): 1482-1513.

[50] Becerril, Héctor A., et al. "Evaluation of solution-processed reduced graphene oxide films as transparent conductors." *ACS nano* 2.3 (2008): 463-470.

[51] Shin, Hyeon−Jin, et al. "Efficient reduction of graphite oxide by sodium borohydride and its effect on electrical conductance." *Advanced Functional Materials* 19.12 (2009): 1987-1992.

[52] Mattevi, Cecilia, et al. "Evolution of electrical, chemical, and structural properties of transparent and conducting chemically derived graphene thin films." *Advanced Functional Materials* 19.16 (2009): 2577.

[53] Parvez, Khaled, et al. "Electrochemically exfoliated graphene as solution-processable, highly conductive electrodes for organic electronics." *ACS nano*7.4 (2013): 3598-3606.

[54] Zhu, Yanwu, et al. "Transparent self-assembled films of reduced graphene oxide platelets." *Applied Physics Letters* 95.10 (2009): 103104.

[55] Nekahi, A., P. H. Marashi, and D. Haghshenas. "Transparent conductive thin film of ultra large reduced graphene oxide monolayers." *Applied Surface Science* 295 (2014): 59-65.

[56] Pei, Songfeng, et al. "Direct reduction of graphene oxide films into highly conductive and flexible graphene films by hydrohalic acids." *Carbon* 48.15 (2010): 4466-4474.

[57] Kumar, Priyank V., Marco Bernardi, and Jeffrey C. Grossman. "The impact of functionalization on the stability, work function, and photoluminescence of reduced graphene oxide." *ACS nano* 7.2 (2013): 1638-1645.

[58] Pei, Songfeng, and Hui-Ming Cheng. "The reduction of graphene oxide."Carbon 50.9 (2012): 3210-3228.